Bo Lin
Smart and Sustainable
Automation Research Laboratory,
Department of Mechanical Engineering,
University of Michigan, G.G. Brown Laboratory,
2350 Hayward,
Ann Arbor, MI 48109
e-mail: bolin@umich.edu

Molong Duan
Smart and Sustainable
Automation Research Laboratory,
Department of Mechanical Engineering,
University of Michigan, G.G. Brown Laboratory,
2350 Hayward,
Ann Arbor, MI 48109
e-mail: molong@umich.edu

Chinedum E. Okwudire[1]
Associate Professor
Mem. ASME
Smart and Sustainable
Automation Research Laboratory,
Department of Mechanical Engineering,
University of Michigan, G.G. Brown Laboratory,
2350 Hayward,
Ann Arbor, MI 48109
e-mail: okwudire@umich.edu

Analytical and Low-Order Numerical Modeling of Ball-to-Ball Contact Friction in Linear Ball Bearings and Ball Screws

Analytical and low-order numerical models are very useful for studying friction behavior of rolling element machine components like ball bearings and ball screws. This is because they provide generalizable insights into friction behavior at much lower computational costs compared with high-order numerical models like finite element analysis (FEA). While analytical and low-order numerical models in the literature are mainly focused on ball-to-groove contact friction, experimental studies have shown that ball-to-ball contact friction is also very important. This is especially true for linear ball bearings/guideways and ball screws which, unlike rotary ball bearings, do not typically make use of caged balls to prevent ball-to-ball contact. Therefore, in this paper, low-order numerical models for ball-to-ball contact friction in linear ball bearings and ball screws are developed. Furthermore, an analytical model for ball-to-ball contact friction in four-point contact linear ball bearing is derived by making simplifications to its low-order numerical model. Compared with ball-to-ball friction predictions from FEA models developed in ANSYS, the proposed numerical models are shown in case studies to be accurate within 7%, while computing at least three orders of magnitude faster. Moreover, case studies are used to demonstrate how the developed models can be used in practice, e.g., for the mitigation of ball-to-ball contact friction in linear ball bearings and the prediction of friction variation during the operation of a ball screw. [DOI: 10.1115/1.4043630]

1 Introduction

Rolling element machine components with balls, such as ball bearings and ball screws, are used in a wide range of machinery to carry load and transmit motion with low friction [1]. Their friction behavior is very important to their functionality, e.g., accuracy, motion smoothness, and service life [1,2], hence it has been studied extensively in the literature. Before the pioneering work of Jones [3] in modeling ball bearing friction in 1959, friction behavior of ball bearings was studied primarily via experiments [1]. While experiments are very useful in characterizing friction behavior, they often do not have the breadth of scope and depth of insight provided by physics-based models; they can also be expensive to carry out, often requiring specialized jigs. Consequently, building on Jones' work, several physics-based models of friction in ball bearings have been proposed [2,4–7]. The typical modeling process is to derive the relative velocity field between each ball-groove contact and obtain frictional force and moment by integrating infinitesimal frictional stress over the contact area; by establishing the quasi-static equilibrium of frictional force and moment, ball motion and friction are solved iteratively. Harris and Kotzalas [5] gave a comprehensive summary of various aspects of friction modeling of ball bearings. Recently, Leblanc and Nelias [6] extended Jones' model from two-point contact to three- and four-point contact ball bearings. Joshi et al. [7] simplified the friction model developed by Leblanc and Nelias [6] for high-load low-speed ball bearings with both two-point contact and four-point contact and validated the simplified model against a specially designed friction torque rig. Halpin and Tran [2] used minimum energy criteria to solve the friction dynamics of four-point contact ball bearings. For ball screws, a different kinematic pattern from ball bearings was found due to the presence of helix [8]. Correspondingly, friction models for ball screws were proposed following the similar process predescribed for ball bearings [9–11]. The beauty of the described models is that they are low-order (from a numerical standpoint) compared with the alternative which is to utilize high-order finite element analysis (FEA) models that incur much larger computational costs [12]. Moreover, low-order models can sometimes be further simplified to yield elegant analytical formulations that provide explicit relationships between friction behavior and system parameters [13,14].

A problem is that the existing low-order numerical and analytical models focus on modeling ball-to-groove contact friction behavior without considering another important source of friction, i.e., ball-to-ball contact friction. Shimoda and Izawa [15] found, via experiments, that friction torque in oscillatory ball screws can be more than twice larger than usual, due to ball-to-ball contact. Ohta et al. [16], by observing loaded balls in the ball track of a linear guideway type ball bearing with a camera, proved that significant frictional force occurs due to ball-to-ball contact. One way to mitigate the friction rising from ball-to-ball contact is to use spacer balls (i.e., smaller-size balls) between adjacent load-carrying balls [15,16]. The spacer balls translate sliding friction between balls into rolling friction, thus mitigating ball-to-ball contact friction. However, the adoption of spacer balls has an obvious drawback, i.e., with the same number of balls, load capacity is reduced by half. Therefore, to maintain the same load capacity, the number of balls needs to be doubled—which increases the size and cost of the machine element. Another way to mitigate ball-to-ball contact is to use cages (or retainers) [17]. While caged balls are commonly adopted in rotary ball bearings, they are not commonly used with linear ball bearings (for the sake of brevity, linear ball bearing will be used in this work to represent both linear ball bearings and linear guideways) and ball screws mainly because of the complexity related to recirculation and the potential reliability issues they pose [17]. Given the significance of ball-to-ball contact friction in machine elements like linear ball bearings and

[1]Corresponding author.

Contributed by the Tribology Division of ASME for publication in the JOURNAL OF TRIBOLOGY. Manuscript received October 24, 2018; final manuscript received April 25, 2019; published online May 17, 2019. Assoc. Editor: Wenzhong Wang.

ball screws, there is a need for low-order numerical or analytical models that consider ball-to-ball contact friction; however, no such works have been found in the literature.

In the preliminary work carried out by the present authors [18], an analytical formula for the linear velocity of balls in four-point contact linear ball bearings was derived. Ball-to-ball contact was shown to take place due to the velocity difference of balls as a result of contact angle deviation. However, the effect of ball-to-ball contact on friction was not investigated, and the study was not extended to ball screws. Therefore, building on the preliminary work [18], the main contributions of this paper are in: (1) developing low-order numerical models for ball-to-ball contact friction in linear ball bearings and ball screws and validating them favorably against FEA models; (2) proposing an analytical model for ball-to-ball contact friction in linear ball bearings, based on the low-order numerical model; and (3) demonstrating how insights gained from the analytical model can be used for mitigation of ball-to-ball contact. Additionally, this paper shows in a case study how the developed low-order models can be used for predicting so-called "friction roughness" (i.e., friction variation) that commonly occurs during the operation of linear ball bearings and ball screws.

The paper is organized as follows: Section 2 focuses on linear ball bearings: ball-to-ball contact friction between two balls and multiple balls is first modeled; an analytical model of ball-to-ball contact is then derived based on simplifying approximations. Following this, case studies are presented to show the effect of ball-to-ball contact on friction and demonstrate how insight gained from the analytical model can be used to mitigate ball-to-ball contact. Finally, the proposed low-order numerical and analytical models are validated against ANSYS FEA. Section 3 then moves to ball screws, starting with ball-to-ball contact modeling followed by FEA validation in ANSYS. Building on the authors' prior work on static load distribution model for ball screws [19], a full friction model of ball screw with ball-to-ball contact is proposed. A simulation-based case study is then presented to show the friction increase and variation in a ball screw mechanism due to ball-to-ball contact.

2 Ball-to-Ball Contact Modeling for Linear Ball Bearings

2.1 Background on Ball Motion and Friction Modeling of a Single Ball. In order to model ball-to-ball contact between multiple balls in a linear ball bearing, a first step is to model the motion and friction of a single ball. There are many friction models in the literature developed for rotary ball bearings [2–6], and the same process applies to linear ball bearings. Here, a brief summary is given.

Without loss of generality, ball motion and friction modeling are presented in the basic module of a four-point contact linear ball bearing as shown in Fig. 1. In the setup, the bottom groove is fixed and the top groove is moving at a constant velocity of magnitude v.

To analyze ball motion and friction, coordinate systems need to be established. Figure 2 depicts the cross section of a single ball in Fig. 1. Define a global coordinate system (CS = {x,y,z}), fixed in space as shown in Fig. 2, with its z-axis passing through the ball center pathway and its xy-plane parallel to the cross section of the raceway. The ball, with radius R_B, is in four-point contact with the BL, BR, TR, and TL (representing bottom/top and left/right) grooves of the raceway. Contact angles β_{BL}, β_{BR}, β_{TR}, and β_{TL} are measured from $\pm y$-axis to the corresponding contact normal in the cross section (see Fig. 2). Local coordinate systems CS_{BL}, CS_{BR}, CS_{TR}, and CS_{TL} are established at the corresponding contact centers such that local z-axes are parallel to the global z-axis and local y-axes lie along the corresponding contact normal, as shown for CS_{BL} in Fig. 2. The contact area is spread over each of the ball-groove contact interface. Since the contact area is relatively small compared with the ball radius, it is assumed to be in the local xz-plane in this work, as shown in Fig. 2 for x_{BL}-z_{BL}.

The movement of the top groove in the global z-direction at constant velocity v makes the ball to translate and rotate. Assume, at quasi-static state, that the ball translates with linear velocity v_B in the global z-direction (i.e., $\mathbf{v}_B = \{0, 0, v_B\}^T$ in vector form) and rotates with $\boldsymbol{\Omega}$ ($= \{\omega_x, \omega_y, 0\}^T$) about an axis passing through the ball center. It is shown that the angular velocity of the ball about the z-axis should always be zero in order for the frictional moment about the z-axis to be balanced [18]. Velocities of any point in the contact area on both ball side and groove side can be expressed based on rigid body kinematics detailed in Ref. [18]. Taking the BL contact interface as an example, the relative velocity between the ball and the BL groove (denoted as $\Delta\mathbf{v}_{BL,B}$) at any point with local coordinates (x_{BL}, z_{BL}) in the contact plane is expressed as

$$\begin{Bmatrix} (\Delta\mathbf{v}_{BL,B})_{BL,x} \\ (\Delta\mathbf{v}_{BL,B})_{BL,z} \end{Bmatrix} = \begin{Bmatrix} (\omega_x \sin\beta_{BL} + \omega_y \cos\beta_{BL}) z_{BL} \\ v_B - (\omega_x \cos\beta_{BL} - \omega_y \sin\beta_{BL}) R_B - (\omega_x \sin\beta_{BL} + \omega_y \cos\beta_{BL}) x_{BL} \end{Bmatrix} \tag{1}$$

Defining

$$\omega_{BL} \triangleq \omega_x \sin\beta_{BL} + \omega_y \cos\beta_{BL}$$
$$c_{BL} \triangleq \frac{v_B - (\omega_x \cos\beta_{BL} - \omega_y \sin\beta_{BL}) R_B}{\omega_{BL}} \tag{2}$$

The relative velocity field in Eq. (1) is rewritten as

$$\begin{Bmatrix} (\Delta\mathbf{v}_{BL,B})_{BL,x} \\ (\Delta\mathbf{v}_{BL,B})_{BL,z} \end{Bmatrix} = \begin{Bmatrix} \omega_{BL} z_{BL} \\ \omega_{BL}(c_{BL} - x_{BL}) \end{Bmatrix} \tag{3}$$

Following the same procedure, the relative velocity fields for the BR, TL, and TR contact areas are also derived as shown in the

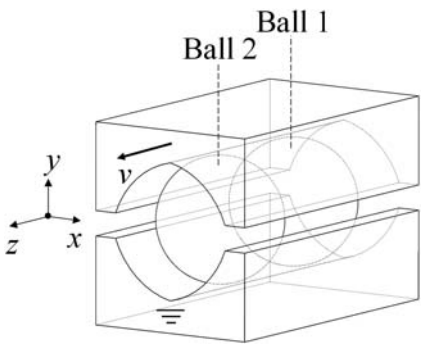

Fig. 1 Basic module of two balls in a four-point contact linear ball bearing

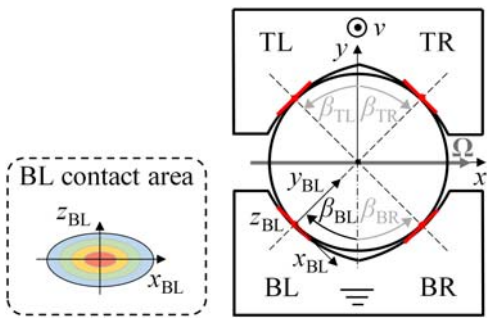

Fig. 2 Geometry and coordinate systems for a four-point contact linear ball bearing

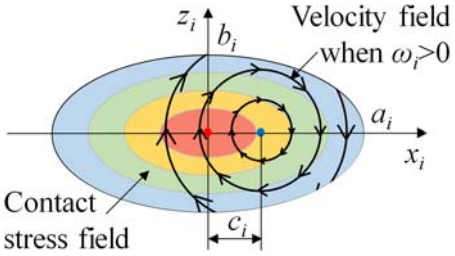

Fig. 3 Contact area and relative velocity field for linear ball bearing

Appendix. The relative velocity fields in the four elliptical contact area (with semi-major axis a_i and semi-minor axis b_i) all take the same general form: they appear as circular contours centered at (c_i, 0) as shown in Fig. 3, with $i \in \{\text{BL, BR, TR, TL}\}$.

Given the relative velocity field over the assumed planar contact area, friction is calculated by double integrating the infinitesimal frictional stress with normal contact stress distribution. It is a standard process that many friction models adopted [2–6]. But with the planar contact area approximation and the velocity field derived in Eq. (3), friction can be analyzed explicitly [18]. Given the symmetry of the contact stress field and velocity field about the x_i-axis in Fig. 3, the frictional force along the x_i-axis is zero. The frictional force $f_{i,z}$ along the z_i-axis, the frictional moment $M_{i,O}$ about the contact center and the frictional loss P_{fi} measured in power are calculated as shown in the Appendix. Since the frictional forces are in the z_i-direction and the frictional moments are about y_i-axes, friction is decoupled from normal contact forces which lie in the xy-plane.

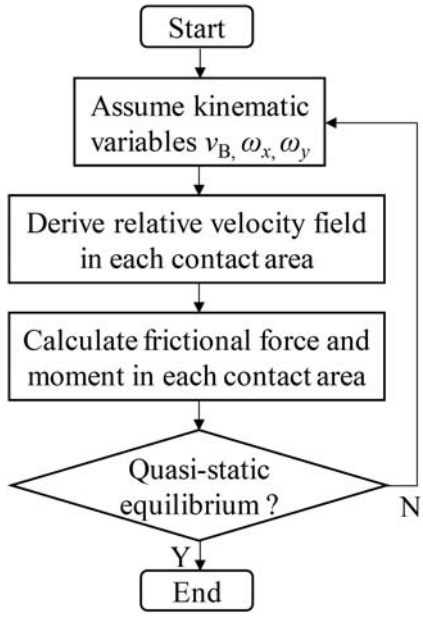

Fig. 4 Flowchart for the solving process of ball motion and friction in linear ball bearing

It is found that gyroscopic effect is negligible at low-speed application [2,7]. Ignoring gyroscopic effect, the ball needs to be in quasi-static equilibrium under frictional forces and moments as

$$\sum \begin{pmatrix} \mathbf{F} \\ \mathbf{M} \end{pmatrix}_0 = \begin{bmatrix} 1 & 1 & 1 & 1 \\ -\cos\beta_{BL} & -\cos\beta_{BR} & \cos\beta_{TR} & \cos\beta_{TL} \\ \sin\beta_{BL} & -\sin\beta_{BR} & -\sin\beta_{TR} & \sin\beta_{TL} \end{bmatrix} \begin{Bmatrix} f_{BL,z} \\ f_{BR,z} \\ f_{TR,z} \\ f_{TL,z} \end{Bmatrix} + \begin{bmatrix} 0 & 0 & 0 & 0 \\ \sin\beta_{BL} & -\sin\beta_{BR} & -\sin\beta_{TR} & \sin\beta_{TL} \\ \cos\beta_{BL} & \cos\beta_{BR} & -\cos\beta_{TR} & -\cos\beta_{TL} \end{bmatrix} \begin{Bmatrix} -M_{BL,O}/R_B \\ -M_{BR,O}/R_B \\ -M_{TR,O}/R_B \\ -M_{TL,O}/R_B \end{Bmatrix} = \begin{Bmatrix} 0 \\ 0 \\ 0 \end{Bmatrix} \tag{4}$$

where the first equation represents the equilibrium of frictional forces in the z-direction. The second and third equations represent equilibrium of frictional moment about the x- and y-axis, respectively, which are normalized by ball radius R_B to be equivalent force equations. It is worth noticing that there is a minus sign before $M_{i,O}$ in Eq. (4), because $M_{i,O}$ is measured about the corresponding $-y_i$-axis as shown in Fig. 3.

With the three equations, the three kinematic variables v_B, ω_x, and ω_y are solved in an iterative process using the *fsolve* function in MATLAB. Maps of frictional force/moment/loss are built beforehand as functions of c_i/a_i according to equations presented in the Appendix. In the solution process, linear interpolation is used to retrieve the values to speed up the calculation instead of performing numerical integration. Upon the solution of kinematic variables, frictional force/moment and loss are determined accordingly. In summary, the process can be described by the flowchart as shown in Fig. 4.

2.2 Low-Order Numerical Model of Ball-to-Ball Contact Friction. The linear velocities of individual balls differ depending on their contact angles and loading conditions. Ball-to-ball contact develops: (1) when the linear velocity $v_{B,10}$ of the ball behind (ball 1 in Fig. 1) is faster than $v_{B,20}$ of the ball in front, i.e., $v_{B,10} > v_{B,20}$ and (2) when the distance between the two ball centers d_{12} is small enough ($d_{12} \le 2R_B$). Notice that "0" in the subscript is used to denote the velocity of individual balls before ball-to-ball contact. After contact, ball-to-ball contact causes the two balls to eventually have the same linear velocity ($v_{B,1} = v_{B,2}$). Because the relative velocities of the two contacting balls at their contact interface are usually of opposite direction, massive sliding friction loss occurs [16]. Since the contact deformations are in the μm-level, the transient process of ball-to-ball contact is ignored and only the quasi-steady states before and after contact are modeled.

After ball-to-ball contact stabilizes (i.e., when $v_{B,1} = v_{B,2}$), the relative velocity at the ball-to-ball contact interface measured on ball 1 is expressed as

$$\begin{Bmatrix} (\Delta \mathbf{v}_{B2B})_x \\ (\Delta \mathbf{v}_{B2B})_y \end{Bmatrix} = \begin{Bmatrix} (\omega_{y,1} + \omega_{y,2})R_B \\ -(\omega_{x,1} + \omega_{x,2})R_B \end{Bmatrix} \tag{5}$$

Denoting the normal contact force in the ball-to-ball contact interface as F_{B2B} (i.e., in the global z-direction), the ball-to-ball contact frictional force in the contact interface parallel to the

xy-plane is

$$\begin{Bmatrix} f_{\mathrm{B2B},x} \\ f_{\mathrm{B2B},y} \end{Bmatrix} = \begin{Bmatrix} -(\Delta\mathbf{v}_{\mathrm{B2B}})_x/|\Delta\mathbf{v}_{\mathrm{B2B}}| \cdot \mu F_{\mathrm{B2B}} \\ -(\Delta\mathbf{v}_{\mathrm{B2B}})_y/|\Delta\mathbf{v}_{\mathrm{B2B}}| \cdot \mu F_{\mathrm{B2B}} \end{Bmatrix}, \quad |\Delta\mathbf{v}_{\mathrm{B2B}}| = \sqrt{(\Delta\mathbf{v}_{\mathrm{B2B}})_x^2 + (\Delta\mathbf{v}_{\mathrm{B2B}})_y^2} \tag{6}$$

where μ represents friction coefficient of metal-to-metal contact. The frictional loss measured in power is

$$P_{f_{\mathrm{B2B}}} = \mu F_{\mathrm{B2B}} |\Delta\mathbf{v}_{\mathrm{B2B}}| \tag{7}$$

It can be proven that there is no relative spin at the ball-to-ball contact interface, otherwise the frictional moment about the z-axis cannot be balanced quasi-statically for each ball. Notice that the ball-to-ball contact frictional forces are parallel to the xy-plane and they should influence the ball-to-groove contact forces in theory. However, due to the small value of μ (around 0.1 according to experimental measurement in Ref. [7]), ball-to-ball contact frictional forces are at least one order of magnitude smaller than the ball-to-groove contact forces. Therefore, it is reasonable to assume that ball-to-groove contact forces are not affected by ball-to-ball contact friction and the calculation of ball-to-ball contact force and friction is decoupled from ball-to-groove contact forces. Based on this assumption, the new quasi-static equilibrium of ball 1 considering ball-to-ball contact force and friction becomes

$$\sum \begin{pmatrix} \mathbf{F} \\ \mathbf{M} \end{pmatrix}_0 + \begin{bmatrix} -1 & 0 & 0 \\ 0 & 0 & -1 \\ 0 & 1 & 0 \end{bmatrix} \begin{Bmatrix} F_{\mathrm{B2B}} \\ f_{\mathrm{B2B},x} \\ f_{\mathrm{B2B},y} \end{Bmatrix} = \begin{Bmatrix} 0 \\ 0 \\ 0 \end{Bmatrix} \tag{8}$$

Note that the last two equations represent the equilibrium of normalized frictional moments. Similar equations hold for ball 2, only that ball-to-ball contact force and friction are in the opposite direction.

Besides satisfying their own quasi-static equilibrium, the two balls need to satisfy ball-to-ball contact conditions: if the two balls are in contact, then they need to move in the same linear velocity at the quasi-static state; otherwise, the ball-to-ball contact force is zero.

$$\begin{cases} v_{\mathrm{B},1} = v_{\mathrm{B},2}, & \text{if } v_{\mathrm{B},10} \geq v_{\mathrm{B},20} \text{ and } d_{12} \leq 2R_{\mathrm{B}} \\ F_{\mathrm{B2B}} = 0, & \text{otherwise} \end{cases} \tag{9}$$

Put together, Eq. (8) for quasi-static equilibrium of ball 1, similar equations for ball 2 and Eq. (9) for ball-to-ball contact, the motion of the two balls and ball-to-ball contact force F_{B2B} are determined iteratively. Upon solution, ball-to-ball contact friction and loss are obtained according to Eqs. (6) and (7).

Ball-to-ball contact between two balls can be generalized to multi-ball-to-ball contact as

$$\begin{cases} \text{Quasi-static equilibrium for ball } j \text{ (similar to Eq. (8))} \\ \text{B2B contact between ball } j \text{ and } j+1: \begin{cases} v_{\mathrm{B},j} = v_{\mathrm{B},(j+1)}, & \text{if } v_{\mathrm{B},j0} \geq v_{\mathrm{B},(j+1)0} \text{ and } d_{j(j+1)} \leq 2R_{\mathrm{B}} \\ F_{\mathrm{B2B},j} = 0, & \text{otherwise} \end{cases} \end{cases} \tag{10}$$

For N_{B} balls in contact, there are three kinematic variables for each of them; in addition, there are $(N_{\mathrm{B}}-1)$ variables for ball-to-ball contact. Accordingly, each ball needs to be in quasi-static equilibrium with three equations, and $(N_{\mathrm{B}}-1)$ equations for ball-to-ball contact condition. In total, there are $4(N_{\mathrm{B}}-1)$ variables and equations, so the multi-ball-to-ball contact problem is solvable. Again, *fsolve* function in MATLAB is adopted to solve the problem.

2.3 Analytical Model of Ball-to-Ball Contact. In the preceding subsection, a low-order numerical model for ball-to-ball contact with iterative solution process was proposed. Wherever possible, it is desirable to have analytical models to gain more insight into the relationship between friction and the associated parameters. This subsection derives analytical formulas for the linear velocity of an individual ball, ball-to-ball contact force and friction in four-point contact linear ball bearings with proper approximations.

2.3.1 Analysis of Frictional Force and Moment. The frictional force $f_{i,z}$ and moment $M_{i,O}$ in each contact area are functions of c_i/a_i, an indicator for the deviation of velocity center from the contact center. Extreme values of $f_{i,z}$ and $M_{i,O}$ are achieved at $c_i/a_i = 0$ as

$$f_{i,z}|_{c_i/a_i=0} = 0$$
$$M_{i,O}|_{c_i/a_i=0} = \frac{3}{8}\mathrm{sgn}(\omega_i)\mu F_i a_i \cdot \mathrm{Ellip}\left(\frac{\sqrt{a_i^2 - b_i^2}}{a_i}\right) \tag{11}$$

where Ellip$(\cdot)$ represents the complete elliptic integral of the second kind. The case of $c_i/a_i = 0$ represents pure spin about the contact center. The other set of extreme values are achieved when $c_i/a_i \to \pm\infty$ as

$$f_{i,z}|_{c_i/a_i\to\pm\infty} = \mp\mathrm{sgn}(\omega_i)\mu F_i$$
$$M_{i,O}|_{c_i/a_i\to\pm\infty} = 0 \tag{12}$$

where pure sliding happens.

The frictional force and moment in each contact area are also affected by b_i/a_i, which is the same for four contact points in a linear ball bearing and is solely determined by the conformity ratio (conf. $= R_{\mathrm{G}}/2R_{\mathrm{B}}$, with R_{G} representing the radius of the cross-sectional groove profile) of the groove [2,6]. To normalize $f_{i,z}$, it is divided by its extreme value $\mathrm{sgn}(\omega_i)\mu F_i$, while $M_{i,O}$ is normalized by dividing the product of $\mathrm{sgn}(\omega_i)\mu F_i$ and moment arm R_{B} in order to make it comparable in magnitude to $f_{i,z}$ in the equations of force and moment equilibrium. The numerical results of normalized $f_{i,z}$ and $M_{i,O}$ as functions of c_i/a_i under four typical conformity ratios of ball bearings are shown in Fig. 5.

Observing from Fig. 5, there is no significant difference among the plots of the four typical conformity ratios, thus they are not distinguished in the discussion. It is observed that the normalized frictional moment is very small compared with the normalized frictional force over a wide range as shown in Fig. 5(*a*). Frictional moment is only comparable with the frictional force when c_i/a_i is very close to zero. When $|c_i/a_i| < 0.5$, $f_{i,z}$ is almost linear with respect to c_i/a_i as shown in Fig. 5(*b*). While in the same region, the change of normalized $M_{i,O}$ is negligible compared with that of $f_{i,z}$. In fact, $|c_i/a_i|$ is usually very small in four-point contact as observed from the results presented in Refs. [6,12]. Small $|c_i/a_i|$ condition breaks down only when there is two-point contact or near two-point contact (i.e., contact forces on one diagonal pair are significantly larger than those on the other pair). Thus, to simplify the analysis for four-point contact, the frictional force is approximated to be linear with respect to c_i/a_i while the frictional moment is approximated to always take its extreme value given in Eq. (11).

2.3.2 Analytical Formula for Ball Velocity. Based on the approximation of the frictional force and moment, an analytical formula for the linear velocity of a single ball can be obtained. It is presented in the authors' preliminary work [18] and is summarized here to provide the necessary background for ball-to-ball contact analysis. To aid the analysis, an additional variable $\Delta\eta_i$ is introduced

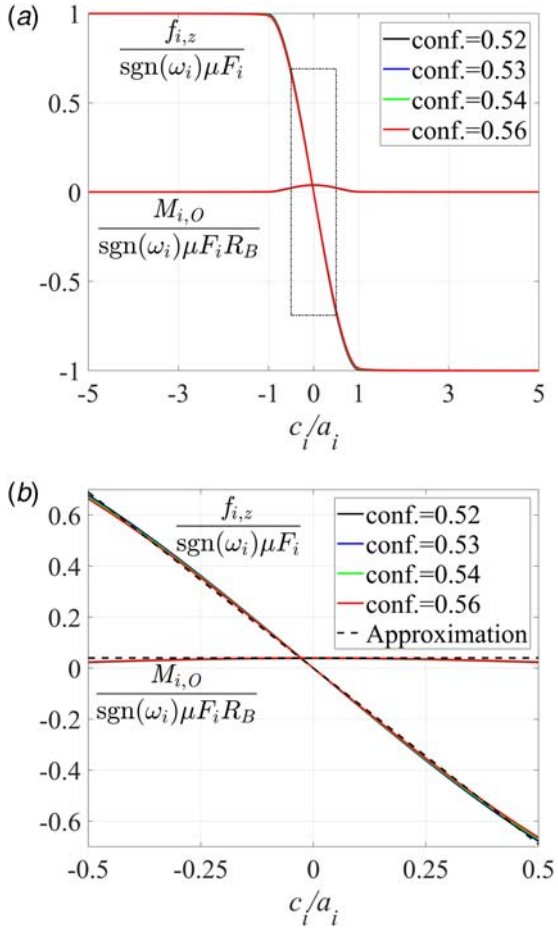

Fig. 5 Frictional force and moment as functions of c_i/a_i: (*a*) full plot and (*b*) zoomed in plot near $c_i/a_i = 0$

for each contact area (see Fig. 6 for $\Delta\eta_{\mathrm{BL}}$), indicating the angular deviation of the velocity center from the contact center in the cross section (i.e., along the semi-major axis of the contact area). Thus,

$$\Delta\eta_i = s_i \frac{c_i}{R_{\mathrm{B}}}, \quad \begin{cases} s_i = 1, & \text{when } i = \mathrm{BR}, \mathrm{TL} \\ s_i = -1, & \text{when } i = \mathrm{BL}, \mathrm{TR} \end{cases} \tag{13}$$

Note that s_i accounts for the sign of $\Delta\eta_i$ in the definition. With the linear approximation, the frictional force becomes

$$f_{i,z} = -\mathrm{sgn}(\omega_i)\mu F_i k_f \frac{c_i}{a_i} = -\mathrm{sgn}(\omega_i)\mu F_i k_f \frac{R_{\mathrm{B}}}{a_i}\frac{\Delta\eta_i}{s_i} \tag{14}$$

Based on the plot in Fig. 5, $k_f = 1.38$ is picked. It is shown in the Appendix that for the linear approximation to be valid, $\Delta\eta_i$ is a small value ($-6.25\ \mathrm{deg} < \Delta\eta_i < 6.25\ \mathrm{deg}$). The length of semi-major axis a_i is related with normal contact force F_i according to Hertzian contact theory [20] as

$$a_i = \Psi R_{\mathrm{B}}^{1/3} F_i^{1/3} \tag{15}$$

where Ψ is a constant determined by the geometry and material properties.

In four-point contact, we have observed that typically $\omega_{\mathrm{BL}} > 0$, $\omega_{\mathrm{BR}} < 0$, $\omega_{\mathrm{TR}} < 0$, and $\omega_{\mathrm{TL}} > 0$. Substituting the approximated frictional force and moment to the quasi-static equilibrium in Eq. (4), it becomes

$$\begin{bmatrix} 1 & 1 & 1 & 1 \\ -\cos\beta_{\mathrm{BL}} & -\cos\beta_{\mathrm{BR}} & \cos\beta_{\mathrm{TR}} & \cos\beta_{\mathrm{TL}} \\ \sin\beta_{\mathrm{BL}} & -\sin\beta_{\mathrm{BR}} & -\sin\beta_{\mathrm{TR}} & \sin\beta_{\mathrm{TL}} \end{bmatrix} \begin{Bmatrix} \frac{k_f}{\Psi}\mu(R_{\mathrm{B}}F_{\mathrm{BL}})^{2/3}\Delta\eta_{\mathrm{BL}} \\ \frac{k_f}{\Psi}\mu(R_{\mathrm{B}}F_{\mathrm{BR}})^{2/3}\Delta\eta_{\mathrm{BR}} \\ -\frac{k_f}{\Psi}\mu(R_{\mathrm{B}}F_{\mathrm{TR}})^{2/3}\Delta\eta_{\mathrm{TR}} \\ -\frac{k_f}{\Psi}\mu(R_{\mathrm{B}}F_{\mathrm{TL}})^{2/3}\Delta\eta_{\mathrm{TL}} \end{Bmatrix} + \begin{bmatrix} 0 & 0 & 0 & 0 \\ \sin\beta_{\mathrm{BL}} & -\sin\beta_{\mathrm{BR}} & -\sin\beta_{\mathrm{TR}} & \sin\beta_{\mathrm{TL}} \\ \cos\beta_{\mathrm{BL}} & \cos\beta_{\mathrm{BR}} & -\cos\beta_{\mathrm{TR}} & -\cos\beta_{\mathrm{TL}} \end{bmatrix} \begin{Bmatrix} -\frac{3}{8}\Psi\,\mathrm{Ellip}\,\mu R_{\mathrm{B}}^{-2/3}F_{\mathrm{BL}}^{4/3} \\ \frac{3}{8}\Psi\,\mathrm{Ellip}\,\mu R_{\mathrm{B}}^{-2/3}F_{\mathrm{BR}}^{4/3} \\ \frac{3}{8}\Psi\,\mathrm{Ellip}\,\mu R_{\mathrm{B}}^{-2/3}F_{\mathrm{TR}}^{4/3} \\ -\frac{3}{8}\Psi\,\mathrm{Ellip}\,\mu R_{\mathrm{B}}^{-2/3}F_{\mathrm{TL}}^{4/3} \end{Bmatrix} = \begin{Bmatrix} 0 \\ 0 \\ 0 \end{Bmatrix} \tag{16}$$

Besides the equilibrium of frictional force and moment presented in Eq. (16), one more relationship comes from the kinematic constraint. In the authors' prior work [13], it was found that the two "zero-velocity lines" that pass through the zero-velocity points (i.e., velocity center c_i) on the same side of the groove (see Fig. 6) are parallel. It still holds true in this work with $\beta_i + \Delta\eta_i$ representing the angle of zero-velocity point, which means that [13]

$$\begin{aligned} &\sin(\beta_{\mathrm{BL}} + \Delta\eta_{\mathrm{BL}} + \beta_{\mathrm{TL}} + \Delta\eta_{\mathrm{TL}}) + \sin(\beta_{\mathrm{BR}} + \Delta\eta_{\mathrm{BR}} - \beta_{\mathrm{TL}} - \Delta\eta_{\mathrm{TL}}) \\ &= \sin(\beta_{\mathrm{BR}} + \Delta\eta_{\mathrm{BR}} + \beta_{\mathrm{TR}} + \Delta\eta_{\mathrm{TR}}) + \sin(\beta_{\mathrm{BL}} + \Delta\eta_{\mathrm{BL}} - \beta_{\mathrm{TR}} - \Delta\eta_{\mathrm{TR}}) \end{aligned} \tag{17}$$

For contact angles β_i, there is a nominal value β_0. However, the actual contact angle deviates from β_0 due to the presence of geometric error and/or misalignment. We define

$$\Delta\beta_i \triangleq \beta_i - \beta_0 \tag{18}$$

where $\Delta\beta_i$ is the contact angle deviation and is usually very small (typically $-3\ \mathrm{deg} < \Delta\beta_i < 3\ \mathrm{deg}$). Under the assumption of small $\Delta\beta_i + \Delta\eta_i$, Eq. (17) is approximated as

$$\begin{aligned} &(\Delta\beta_{\mathrm{BL}} + \Delta\eta_{\mathrm{BL}}) + (\Delta\beta_{\mathrm{TL}} + \Delta\eta_{\mathrm{TL}}) - (\Delta\beta_{\mathrm{BR}} + \Delta\eta_{\mathrm{BR}}) \\ &- (\Delta\beta_{\mathrm{TR}} + \Delta\eta_{\mathrm{TR}}) = 0 \end{aligned} \tag{19}$$

Putting Eqs. (16) and (19) together, the angular deviation $\Delta\eta_i$ can be analytically determined.

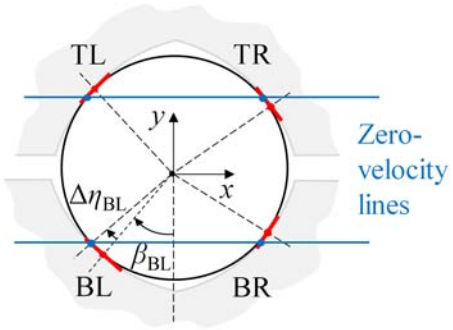

Fig. 6 Angular deviation of velocity center from contact center

The linear velocity of the ball center is formulated as [13]

$$v_B = \frac{\sin(\beta_{BL} + \Delta\eta_{BL} + \beta_{BR} + \Delta\eta_{BR})v}{\sin(\beta_{BL} + \Delta\eta_{BL} + \beta_{BR} + \Delta\eta_{BR}) + \sin(\beta_{BL} + \Delta\eta_{BL} + \beta_{TL} + \Delta\eta_{TL}) + \sin(\beta_{BR} + \Delta\eta_{BR} - \beta_{TL} - \Delta\eta_{TL})} \tag{20}$$

With small $\Delta\beta_i + \Delta\eta_i$ approximation, Eq. (20) reduces to

$$v_B \approx \left(1 + \underbrace{(1 - \cos(2\beta_0))\frac{-\Delta\beta_{BR} - \Delta\eta_{BR} + \Delta\beta_{TL} + \Delta\eta_{TL}}{2}}_{\varepsilon}\right)\frac{v}{2} \tag{21}$$

where ε is the deviation of ball center velocity from the nominal ball center velocity $v/2$. Substituting the solution of $\Delta\eta_i$ from Eqs. (16) and (19) into Eq. (21), ε is obtained as a function of four contact angle deviations $\Delta\beta_i$ and four normal contact forces F_i. The expression for ε is still cumbersome, but there is one more approximation to be made. Since the contact angle deviations $\Delta\beta_i$ are small, the contact forces on the same diagonal pair (i.e., BL and TR pair and BR and TL pair) are very close under external load in four-point contact [12]. With the approximation that $F_{BL} \approx F_{TR} \triangleq F_U$ and $F_{BR} \approx F_{TL} \triangleq F_D$, the ball center velocity deviation is simplified to

$$\varepsilon \approx (1 - \cos(2\beta_0))\frac{(-\Delta\beta_{BL} + \Delta\beta_{TR})F_U^{2/3} + (-\Delta\beta_{BR} + \Delta\beta_{TL})F_D^{2/3}}{2(F_U^{2/3} + F_D^{2/3})} \tag{22}$$

This formula explicitly shows the effect of contact angle deviations and contact forces on the ball linear velocity deviation ε. A few insights from the analytical formula are (1) ball center velocity deviation differs under different contact angle deviations and loading conditions; (2) ball linear velocity is not affected by external loading in the absence of contact angle deviations; and (3) ball linear velocity is not affected by external loading under certain combinations of contact angle deviations, i.e., when $\Delta\beta_{BL} = \Delta\beta_{TR}$ and $\Delta\beta_{BR} = \Delta\beta_{TL}$.

Compared with the low-order friction models described in Sec. 2.1, three major approximations are made in the analytical derivation presented above: (i) $\omega_{BL} > 0$, $\omega_{BR} < 0$, $\omega_{TR} < 0$, and $\omega_{TL} > 0$; (ii) $\Delta\beta_i + \Delta\eta_i$ for each contact point is small; and (iii) contact forces on the same diagonal pair are approximated to be the same. Four-point contact is a necessary condition for all three approximations. If there are only two contact points or near two-point contact (i.e., contact forces on one diagonal pair are significantly larger than those on the other pair), the angular deviation of velocity center from contact center $\Delta\eta_i$ becomes large so that small $\Delta\beta_i + \Delta\eta_i$ assumption becomes invalid; approximations (i) and (iii) also become obsolete.

2.3.3 Analytical Formula for Ball-to-Ball Contact Force and Friction. So far, the analytical formula for ball center velocity of individual balls are obtained. According to the ball-to-ball contact model, if the two balls in Fig. 1 with $v_{B,10} = (1 + \varepsilon_1)v/2$ and $v_{B,20} = (1 + \varepsilon_2)v/2$ satisfy $\varepsilon_1 > \varepsilon_2$, ball-to-ball contact will happen when the distance between the two ball centers d_{12} is small enough. Ball-to-ball contact force and friction change the equilibrium of each ball. On top of $\Delta\eta_i$, assume that the additional angular contact deviation of the velocity center is $\Delta\zeta_i$ for each contact area due to ball-to-ball contact. If the deviation still falls in the linear region of the frictional force in Fig. 5, the frictional force is approximated as

$$f_{i,z} = -\text{sgn}(\omega_i)\mu F_i k_f \frac{R_B}{a_i}\frac{\Delta\eta_i + \Delta\zeta_i}{s_i} \tag{23}$$

and the frictional moment is still approximated to take its maximum value given in Eq. (11). The new quasi-static equilibrium of ball 1 considering ball-to-ball contact force becomes

$$\begin{bmatrix} 1 & 1 & 1 & 1 \\ -\cos\beta_{BL} & -\cos\beta_{BR} & \cos\beta_{TR} & \cos\beta_{TL} \\ \sin\beta_{BL} & -\sin\beta_{BR} & -\sin\beta_{TR} & \sin\beta_{TL} \end{bmatrix} \begin{Bmatrix} \frac{k_f}{\Psi}\mu(R_B F_{BL})^{2/3}(\Delta\eta_{BL} + \Delta\zeta_{BL}) \\ \frac{k_f}{\Psi}\mu(R_B F_{BR})^{2/3}(\Delta\eta_{BR} + \Delta\zeta_{BR}) \\ -\frac{k_f}{\Psi}\mu(R_B F_{TR})^{2/3}(\Delta\eta_{TR} + \Delta\zeta_{TR}) \\ -\frac{k_f}{\Psi}\mu(R_B F_{TL})^{2/3}(\Delta\eta_{TL} + \Delta\zeta_{TL}) \end{Bmatrix} + \begin{bmatrix} 0 & 0 & 0 & 0 \\ \sin\beta_{BL} & -\sin\beta_{BR} & -\sin\beta_{TR} & \sin\beta_{TL} \\ \cos\beta_{BL} & \cos\beta_{BR} & -\cos\beta_{TR} & -\cos\beta_{TL} \end{bmatrix} \begin{Bmatrix} -\frac{3}{8}\Psi\,\text{Ellip}\,\mu R_B^{-2/3}F_{BL}^{4/3} \\ \frac{3}{8}\Psi\,\text{Ellip}\,\mu R_B^{-2/3}F_{BR}^{4/3} \\ \frac{3}{8}\Psi\,\text{Ellip}\,\mu R_B^{-2/3}F_{TR}^{4/3} \\ -\frac{3}{8}\Psi\,\text{Ellip}\,\mu R_B^{-2/3}F_{TL}^{4/3} \end{Bmatrix} = \begin{Bmatrix} F_{B2B} \\ 0 \\ 0 \end{Bmatrix} \tag{24}$$

Note here that the frictional force at ball-to-ball contact interface is not included in the equations, which is a reasonable approximation because ball-to-ball frictional forces are at least one order of magnitude smaller than ball-to-ball contact force. Subtracting Eq. (16), Eq. (24) becomes

$$\begin{bmatrix} 1 & 1 & 1 & 1 \\ -\cos\beta_{BL} & -\cos\beta_{BR} & \cos\beta_{TR} & \cos\beta_{TL} \\ \sin\beta_{BL} & -\sin\beta_{BR} & -\sin\beta_{TR} & \sin\beta_{TL} \end{bmatrix} \times \begin{Bmatrix} \frac{k_f}{\Psi}\mu(R_B F_{BL})^{2/3}\Delta\zeta_{BL} \\ \frac{k_f}{\Psi}\mu(R_B F_{BR})^{2/3}\Delta\zeta_{BR} \\ -\frac{k_f}{\Psi}\mu(R_B F_{TR})^{2/3}\Delta\zeta_{TR} \\ -\frac{k_f}{\Psi}\mu(R_B F_{TL})^{2/3}\Delta\zeta_{TL} \end{Bmatrix} = \begin{Bmatrix} F_{B2B} \\ 0 \\ 0 \end{Bmatrix} \tag{25}$$

which relates $\Delta\zeta_i$ to ball-to-ball contact force F_{B2B}.

With the additional angular deviation $\Delta\zeta_i$, the ball still needs to satisfy kinematic constraint similar to Eq. (19) as

$$(\Delta\beta_{BL} + \Delta\eta_{BL} + \Delta\zeta_{BL}) + (\Delta\beta_{TL} + \Delta\eta_{TL} + \Delta\zeta_{TL}) - (\Delta\beta_{BR} + \Delta\eta_{BR} + \Delta\zeta_{BR}) - (\Delta\beta_{TR} + \Delta\eta_{TR} + \Delta\zeta_{TR}) = 0 \tag{26}$$

Subtracting Eq. (19), Eq. (26) becomes

$$\Delta\zeta_{BL} + \Delta\zeta_{TL} - \Delta\zeta_{BR} - \Delta\zeta_{TR} = 0 \tag{27}$$

The new velocity of the ball is expressed similar to Eq. (21) as

$$v_B \approx \left(1 + \underbrace{(1-\cos(2\beta_0))\frac{-\Delta\beta_{BR} - \Delta\eta_{BR} + \Delta\beta_{TL} + \Delta\eta_{TL}}{2}}_{\varepsilon} + \underbrace{(1-\cos(2\beta_0))\frac{-\Delta\zeta_{BR} + \Delta\zeta_{TL}}{2}}_{\Delta\varepsilon} \right)\frac{v}{2} \tag{28}$$

Let us denote the additional velocity deviation caused by ball-to-ball contact as $\Delta\varepsilon_1$ and $\Delta\varepsilon_2$, respectively. Two contacting balls need to have the same velocity at quasi-static states, thus

$$v_{B,1} = (1+\varepsilon_1+\Delta\varepsilon_1)v/2 = v_{B,2} = (1+\varepsilon_2+\Delta\varepsilon_2)v/2 \quad \text{or} \quad \varepsilon_1 + \Delta\varepsilon_1 = \varepsilon_2 + \Delta\varepsilon_2 \tag{29}$$

Like the approximation made in Sec. 2.3.2, contact forces on the same diagonal pair are very close under external loading. So, the following approximation is made: $F_{BL,1} \approx F_{TR,1} \triangleq F_{1U}$ and $F_{BR,1} \approx F_{TL,1} \triangleq F_{1D}$, $F_{BL,2} \approx F_{TR,2} \triangleq F_{2U}$ and $F_{BR,2} \approx F_{TL,2} \triangleq F_{2D}$ with 1 and 2 in subscript indicating ball 1 and ball 2, respectively. Putting together Eqs. (25), (27), and (28) for ball 1, the similar set of equations for ball 2 and Eq. (29) for ball-to-ball contact, the ball-to-ball contact force F_{B2B} is analytically determined as

$$F_{B2B} = \frac{2k_f\mu}{\Psi(1-\cos(2\beta_0))} R_B^{2/3} \frac{(F_{1U}^{2/3}+F_{1D}^{2/3})(F_{2U}^{2/3}+F_{2D}^{2/3})}{(F_{1U}^{2/3}+F_{1D}^{2/3})+(F_{2U}^{2/3}+F_{2D}^{2/3})}(\varepsilon_1-\varepsilon_2), \quad \text{if } \varepsilon_1 > \varepsilon_2 \text{ and } d_{12} \le 2R_B \tag{30}$$

The analytical formula for ball-to-ball contact force shows that ball-to-ball contact force is proportional to the velocity difference between the two balls. It is also affected by the normal contact loads on the two balls, friction coefficient and constants related to Hertzian contact.

At the ball-to-ball contact interface of four-point contact linear ball bearings, the relative velocity (i.e., sliding velocity) of the two balls can be approximated as

$$|\Delta\mathbf{v}_{B2B}| = \frac{v}{\cos\beta_0} \tag{31}$$

by assuming both balls rotate about x-axis with nominal contact angle β_0. It is observed to be a reasonable approximation in typical four-point contact linear ball bearing. As a result, the sliding friction loss measured in power in Eq. (7) due to ball-to-ball contact friction is explicitly expressed as

$$P_{fB2B} = \mu F_{B2B}|\Delta\mathbf{v}_{B2B}| = \mu F_{B2B}\frac{v}{\cos\beta_0} \tag{32}$$

2.4 Case Studies

2.4.1 Effect of Ball-to-Ball Contact on Friction. To show the effect of ball-to-ball contact on friction and compare the derived analytical formulas to the proposed low-order numerical model, a case study is conducted in the setup as shown in Fig. 7. Note that the same setup was used in the authors' preliminary work [18] to study the velocity difference of balls. In the setup, nominal contact angle β_0 is set to be 45 deg; contact angle deviation θ (<3 deg), induced by manufacturing error and/or misalignment, only takes place on the bottom groove (usually a long rail). External loading is represented by N_x and N_y applied to the top groove. It is

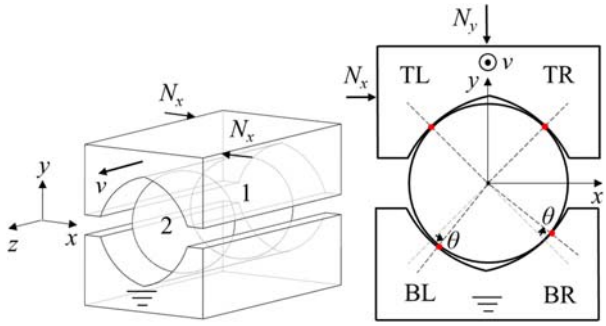

Fig. 7 Contact angle deviations and external loading conditions in the case study

assumed that the same N_y is applied to ball 1 and ball 2 but N_x on the two balls are of opposite direction. This kind of loading condition represents a yaw moment applied to the top groove, which accelerates ball-to-ball contact [16]. According to the definition of contact angle deviations in this work, $\Delta\beta_{BL} = -\theta$, $\Delta\beta_{BR} = \theta$, and $\Delta\beta_{TL} = \Delta\beta_{TR} = 0$. Since the contact angle deviations are small, it is reasonable to approximate the four contact forces as $F_{BL,1} \approx F_{TR,1} \triangleq F_{1U} = \sqrt{2}/2(N_y - N_x)$, $F_{BR,1} \approx F_{TL,1} \triangleq F_{1D} = \sqrt{2}/2(N_y + N_x)$, $F_{BL,2} \approx F_{TR,2} \triangleq F_{2U} = \sqrt{2}/2(N_y + N_x)$, and $F_{BR,2} \approx F_{TL,2} \triangleq F_{2D} = \sqrt{2}/2(N_y - N_x)$. Define $\rho = N_x/N_y$ as the side force ratio and substitute all the parameters into Eq. (22), velocity deviation of the two balls from nominal value is formulated as

$$\varepsilon_1 \approx \frac{\theta F_{1U}^{2/3} - \theta F_{1D}^{2/3}}{2(F_{1U}^{2/3}+F_{1D}^{2/3})} = \frac{\left(1-\left(\frac{1+\rho}{1-\rho}\right)^{2/3}\right)}{\left(1+\left(\frac{1+\rho}{1-\rho}\right)^{2/3}\right)}\frac{\theta}{2}$$
$$\varepsilon_2 \approx \frac{\theta F_{2U}^{2/3} - \theta F_{2D}^{2/3}}{2(F_{2U}^{2/3}+F_{2D}^{2/3})} = -\frac{\left(1-\left(\frac{1+\rho}{1-\rho}\right)^{2/3}\right)}{\left(1+\left(\frac{1+\rho}{1-\rho}\right)^{2/3}\right)}\frac{\theta}{2} \tag{33}$$

Since the loading conditions on the two balls are centrally symmetric, the velocity deviations of the two balls are of opposite sign. Thus, the velocity difference of the two balls, $\varepsilon_1 - \varepsilon_2$, is twice the velocity deviation of a single ball.

Parameters used in the case study are shown in Table 1.

The velocity difference $(\varepsilon_1 - \varepsilon_2)$ of the two balls predicted by the low-order numerical model as a function of θ and ρ is shown in Fig. 8(*a*). As the magnitude of the contact angle deviation $|\theta|$ increases, the velocity difference of the two balls also increases; the same trend is observed for the side force ratio ρ. Results of $(\varepsilon_1 - \varepsilon_2)$ based on the analytical formulas derived in Eq. (33) are shown in Fig. 8(*b*), which are observed to match with the proposed low-order numerical model (see Fig. 8(*a*)) closely. The difference of

Table 1 Parameters for the linear ball bearing case studies

Parameter (symbol)	Value (unit)
Ball radius (R_B)	5 (mm)
Conformity ratio of groove (conf.)	0.56
Constant related to the semi-major axis length (Ψ)	5.307×10^{-4} $((m^2/N)^{1/3})$
Vertical force on each ball (N_y)	100 (N)
Velocity of the top groove (v)	10 (mm/s)
Friction coefficient of metal-to-metal contact (μ)	0.1
Young's modulus	2.1×10^{11} (N/m^2)
Poisson's ratio	0.28

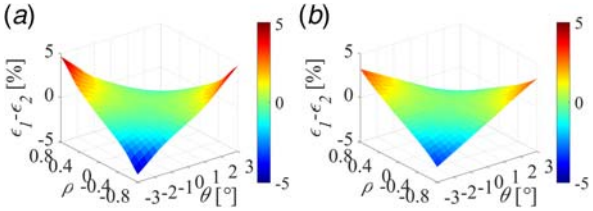

Fig. 8 Velocity difference of two balls as functions of side force ratio and contact angle deviation: (*a*) low-order numerical model and (*b*) analytical formula

the low-order numerical model and the analytical model only becomes noticeable when $|\rho|$ and $|\theta|$ are large. Large $|\rho|$ and $|\theta|$ are exactly where approximations summarized at the end of Sec. 2.3.2 for the analytical formula of velocity deviation fails; four-point contact tends to be (near) two-point contact when $|\rho|$ is large, thus the small $\Delta\beta_i + \Delta\eta_i$ assumption becomes untenable, making the analytical formula inaccurate.

Ball-to-ball contact force and additional friction loss based on the proposed low-order numerical model and the derived analytical formulas are presented in Fig. 9. Ball-to-ball contact only happens when $\varepsilon_1 - \varepsilon_2 > 0$; otherwise, the two balls depart from each other instead of approaching and there is zero ball-to-ball contact force as shown in Figs. 9(*a*) and 9(*b*). For the nonzero contact force region, ball-to-ball contact force F_{B2B} increases with increasing $|\rho|$ and $|\theta|$; so are the total friction loss (with ball-to-ball friction loss $P_{f\mathrm{B2B}}$) versus baseline friction loss (ball-to-groove friction loss P_f). The difference between $F_{\mathrm{B2B}}/P_{f\mathrm{B2B}}$ predicted by the low-order numerical model in Figs. 9(*a*) and 9(*c*) and by the analytical formula in Figs. 9(*b*) and 9(*d*) again only becomes noticeable at large $|\rho|$ and $|\theta|$ region. Since the analytical formulas in Eq. (30) for F_{B2B} and Eq. (32) for $P_{f\mathrm{B2B}}$ are both linear functions of $(\varepsilon_1 - \varepsilon_2)$, the difference in $(\varepsilon_1 - \varepsilon_2)$ calculation shown in Fig. 8 carries over in the calculation of F_{B2B} and P_{fB2B} here. But overall, the analytical formula still predicts ball-to-ball contact force and additional friction loss very well compared with the low-order numerical model. Ball-to-ball contact gives rise to significant increase of friction: the additional friction loss from ball-to-ball contact contributes to more than 185.2% increase compared with the baseline friction (i.e., ball-to-groove contact) in the worst-case scenario according to the low-order numerical model as shown in Fig. 9(*c*).

2.4.2 Using the Analytical Model to Mitigate Ball-to-Ball Contact. Ball-to-ball contact gives rise to significant friction increase as shown in Sec. 2.4.1. Since ball-to-ball contact develops quickly, there is a significant friction variation. Thus, it is desirable to avoid or at least mitigate ball-to-ball contact.

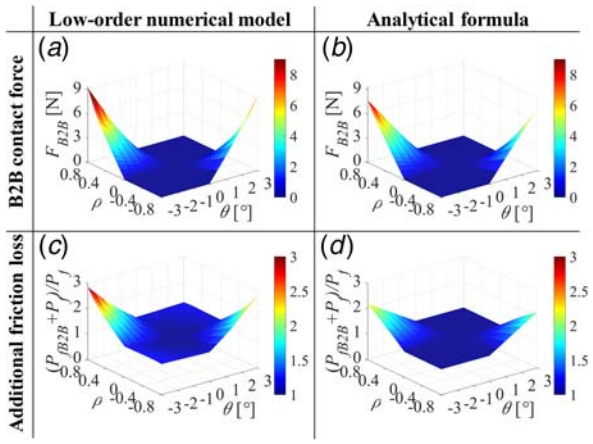

Fig. 9 Ball-to-ball contact forces and friction loss as functions of side force ratio and contact angle deviation

Table 2 Contact angle deviations and velocity deviation of balls in four-point contact linear ball bearings

	Contact angle deviations ($-\Delta\beta_{\mathrm{BL}} = \Delta\beta_{\mathrm{BR}} = \theta =$ 2 deg)		Velocity deviation		
	$\Delta\beta_{\mathrm{TR}}$	$\Delta\beta_{\mathrm{TL}}$		Low-order numerical model (%)	Analytical formula (%)
Case (a)	0	0	ε_1	0.87	0.75
			ε_2	−0.79	−0.75
Case (b)	$-\theta$	θ	ε_1	0	0
			ε_2	0	0

Take a particular case, for example, with $\theta = 2$ deg and $\rho = -0.6$ in Sec. 2.4.1 setup, the two balls have different velocities summarized as case (a) in Table 2. The two balls will develop ball-to-ball contact since ball 1 is moving faster than ball 2. Figure 10(*a*) shows the simulated relative displacement of the two balls using the velocity calculated based on the analytical formulas in Eq. (33), when the initial gap between the two balls is $0.1R_{\mathrm{B}}$. The insight gained from the analytical formula for velocity deviation of balls can be used to mitigate ball-to-ball contact by reducing the velocity difference of balls. Given the contact angle deviations on the bottom groove (usually a long rail), if the contact angle deviations on the top groove (short and sturdy carriage) can be controlled or mated in the manufacturing or assembly processes, the velocity difference of balls can be minimized and ball-to-ball contact can be mitigated. From Eq. (22), it is found that if $\Delta\beta_{\mathrm{TR}} = \Delta\beta_{\mathrm{BL}}$ and $\Delta\beta_{\mathrm{TL}} = \Delta\beta_{\mathrm{BR}}$, then the velocity deviation is always zero irrespective of external loading. This optimized design is simulated with the results shown in Table 2 as case (b) and plotted in Fig. 10(*b*), the two balls remain constant distance because of the optimized design. This highlights the benefit of the proposed analytical formula—it provides explicit relationships between variables and parameters that can be used to guide analysis and design optimization.

2.5 Validation by Finite Element Analysis in ANSYS. In order to validate the low-order numerical model and analytical model of ball-to-ball contact, and to show the validity of using the insight gained from analytical model to mitigate ball-to-ball contact, the results for cases (a) and (b) in Sec. 2.4.2 are compared with those from FEA in ANSYS.

As a benchmark, dynamic simulation of ball-to-ball contact in a linear ball bearing is conducted in ANSYS Workbench 16.2. The model of two balls in contact with two rails is shown in Fig. 11 with mesh. Based on the guidelines provided by ANSYS [21], the ball surface is set as the contact surface, while the groove surface

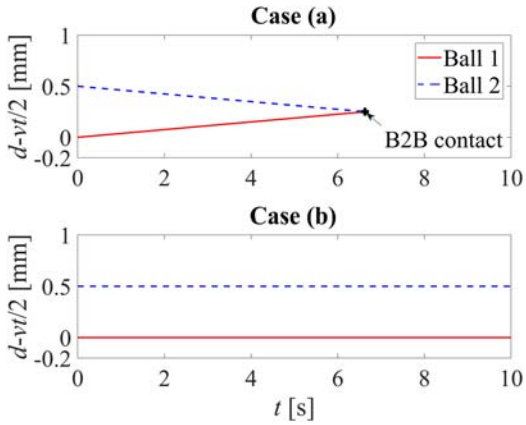

Fig. 10 Example of ball-to-ball contact and its avoidance by optimized design

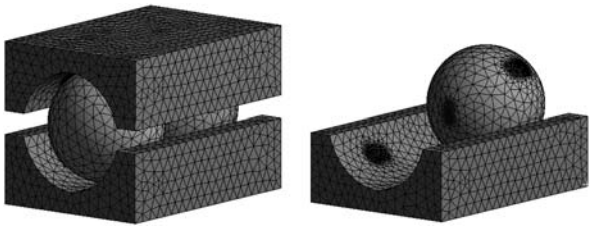

Fig. 11 Mesh for linear ball bearing in ANSYS

is set as the target surface. For the ball-to-ball contact interface, ball 1 is set as target surface while ball 2 is set as the contact surface. All the ball-to-groove and ball-to-ball contact interfaces are set as frictional contact with 0.1 friction coefficient. Augmented Lagrange contact formulations are used for the contact interfaces as recommended by ANSYS because of its robustness and flexibility [21]. All the parts are meshed with tetrahedral elements. It is a common practice to make mesh refinement around the contact region while using coarse mesh elsewhere to reduce the overall number of elements. Here, a mesh refinement technique in ANSYS Workbench called the body of influence is used. The fine mesh is set to be of size 0.13 mm and the coarse mesh of size 1 mm, giving the FE model 294,114 elements in total. Mesh refinement of size 0.13 mm is picked after mesh sensitivity analysis. The bottom groove is fixed and the top groove is made to move at 10 mm/s. Yaw moment of 600 N·mm is applied to create the loading condition in Sec. 2.4.2. The two balls are placed at an initial distance of 1 μm to accelerate ball-to-ball contact such that the top rail does not move out of the mesh-refined area. A total simulation time of 0.1 s is split into ten time steps to simulate the dynamic process from no ball-to-ball contact to the development of ball-to-ball contact and finally stabilized ball-to-ball contact. The force convergence tolerance is set to be 0.1% to balance accuracy and computational efficiency. The other settings in the finite element model are left as default. The solver type is also program-controlled, and it was found out that preconditioned conjugate gradient solver is adopted. Upon solution, the steady-state ball-to-ball contact force is extracted from the FEA result using the reaction force probe.

The ball-to-ball contact force results are compared in Table 3. From the results of case (a), it can be observed that ball-to-ball contact force predicted by the low-order numerical model matches very well to that of ANSYS FEA, with only 1.26% difference. However, the result based on the analytical formula shows a larger error because of the approximations made in the derivation. But the error is still within 6%, which is acceptable. For case (b), ANSYS FEA result shows that the ball-to-ball contact does not happen just as analytical insight predicted, thus the insight gained from the analytical model for ball-to-ball contact mitigation is also validated in ANSYS FEA. Given the accuracy of the proposed low-order numerical model and analytical formula compared with the ANSYS FEA, it is of interest to compare their computational time. As shown in Table 3, the low-order numerical model is three orders of magnitude faster than ANSYS FEA, while analytical formula with explicit form is another two orders of magnitude faster. The proposed low-order model and analytical formula for ball-to-ball contact are therefore computationally much less expensive than the ANSYS FEA model with comparable accuracy, thus is much more desirable, e.g., for use in parametric studies and optimal design of linear ball bearings.

Table 3 Comparison of ball-to-ball contact forces and computational time based on the proposed models and ANSYS FEA for linear ball bearing[a]

		Low-order numerical model	Analytical formula	ANSYS FEA
B2B contact force (N)	Case (a)	4.01	3.74	3.96
	Case (b)	0	0	0
Computation time	Case (a)	0.74 s	6.67 ms	5.11 h
	Case (b)	1.46 s	5.54 ms	3.51 h

[a]All models are run on a desktop computer with Intel(R) Core(TM) i7-3770 CPU of 3.40 GHz and 16 GB RAM.

3 Ball-to-Ball Contact Modeling for Ball Screws

In this section, ball-to-ball contact modeling for linear ball bearings presented in Sec. 2 is generalized to ball screws.

3.1 Ball Motion and Friction Modeling for a Single Ball.

Just like in linear ball bearings, modeling ball motion and friction of a single ball in ball screw is the first step toward modeling ball-to-ball contact. A single-start, right-handed, Gothic-arch-groove-type ball screw with a single ball nut is considered in this work. Without loss of generality, ball motion and friction modeling is presented using a two-ball module of a four-point contact ball screw as shown in Fig. 12. The global coordinate system (CS = $\{x, y, z\}$) is fixed to the screw shaft with its z-axis pointing along the axis of the screw shaft as shown in Fig. 12(*a*). Relative to CS, the inner groove of the two-ball module (representing the screw shaft) in Fig. 12(*b*), is not moving, while the outer groove representing the ball nut is rotating with angular velocity ω_N about the z-axis and at the same time translating at v_N along the z-axis because of the helix. According to the kinematic relationship,

$$v_N = \bar{r}_g \omega_N, \quad \bar{r}_g = \frac{\bar{p}}{2\pi} \tag{34}$$

where $\bar{r}_g$ is the nominal gear ratio and $\bar{p}$ represents the nominal lead of the ball screw.

The locus of points lying on the nominal ball center pathway relative to the origin of CS is expressed as

$$\bar{\mathbf{q}}_B(\varphi) = \begin{Bmatrix} \bar{R}_P \cos\varphi \\ \bar{R}_P \sin\varphi \\ \bar{r}_g \varphi \end{Bmatrix} \tag{35}$$

where φ is the angular distance traversed along the nominal ball center pathway starting from the x-axis to the ball location of interest on the screw (φ is referred to as azimuth angle in this work for the sake of simplicity). $\bar{R}_P$ is the nominal pitch circle radius of the ball screw. Ignoring effects of elastic deformations and geometric errors on the grooves, the ball center velocity in the global coordinate system CS is expressed as

$$\mathbf{v}_B(\varphi) = \begin{Bmatrix} -\bar{R}_P \sin\varphi\omega_B \\ \bar{R}_P \cos\varphi\omega_B \\ \bar{r}_g \omega_B \end{Bmatrix} \tag{36}$$

where ω_B is the orbiting angular velocity of the ball about the ball screw axis.

A moving coordinate system $CS_3 = \{x_3, y_3, z_3\}$, with its origin on the nominal ball center pathway, is established such that its y_3-axis is tangent to the helical path and its x_3-axis points along the radial line from screw axis to nominal ball center as shown in Fig. 12(*a*). Figure 13 shows the cross-sectional profile of the ball screw in the

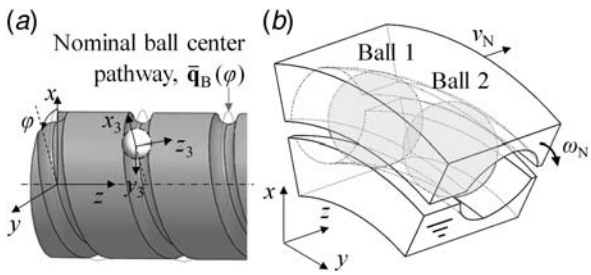

Fig. 12 (*a*) Nominal ball center pathway (helix) and coordinate systems of ball screw and (*b*) two-ball module in ball screw

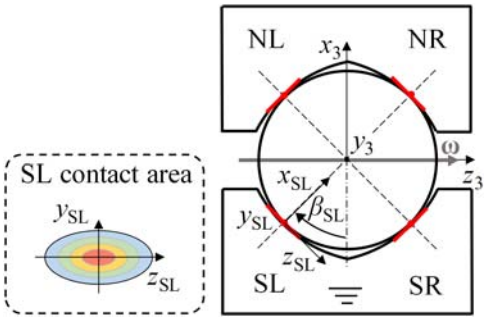

Fig. 13 Geometry and coordinate systems for a four-point contact ball screw

z_3-x_3 plane. A ball, with radius R_B, is in four-point contact with SL, SR, NR, and NL (representing screw/nut and left/right) grooves. Focusing on the SL (screw left) portion of the groove, contact angles β_{SL} are measured from $-x_3$-axis to the contact normal in the cross section. Contact coordinate system CS_{SL} is established at the contact center such that the y_{SL}-axis is parallel to the y_3-axis and the x_{SL}-axis lies along the contact normal as shown in Fig. 13. Similar to linear ball bearings, the contact area is assumed to be in the local $z_{SL}y_{SL}$-plane in this work, as shown in Fig. 13, since the contact area is relatively small compared with the ball radius.

Besides the gross motion, the ball also rotates about its own axis. Assume that the ball is moving at $\boldsymbol{\omega} = [\omega_x, \omega_y, \omega_z]^T$ measured from the local coordinate system CS_3 about an axis passing through the ball center. Velocities of any point in the contact area on both ball side and groove side can be determined based on rigid body kinematics. Focusing on the SL contact area, $\mathbf{q}_{SL}$ is defined as the vector from the ball center to the SL contact center and is given in the local coordinate system CS_3 as

$$\mathbf{q}_{SL} = \begin{Bmatrix} -R_B \cos\beta_{SL} \\ 0 \\ -R_B \sin\beta_{SL} \end{Bmatrix} \tag{37}$$

For any point with local coordinates $(y_{SL}, z_{SL})^T$ in the contact area, its position $\mathbf{q}_{SL,B}$ in CS_3 is

$$\mathbf{q}_{SL,B} = \mathbf{q}_{SL} + \mathbf{T}_{CS_3\text{-}CS_{SL}}[0,\ y_{SL},\ z_{SL}]^T \tag{38}$$

where $\mathbf{T}_{CS3\text{-}CSSL}$ is the transformation matrix from CS_{SL} to CS_3 given by

$$\mathbf{T}_{CS_3\text{-}CS_{SL}} = \begin{bmatrix} \cos\beta_{SL} & 0 & -\sin\beta_{SL} \\ 0 & 1 & 0 \\ \sin\beta_{SL} & 0 & \cos\beta_{SL} \end{bmatrix} \tag{39}$$

The velocity at the SL contact area on the ball side expressed in the global coordinate system CS is

$$\mathbf{v}_{SL,B} = \mathbf{T}_{CS\text{-}CS_3}(\boldsymbol{\omega} \times \mathbf{q}_{SL,B}) + \dot{\mathbf{T}}_{CS\text{-}CS_3}\mathbf{q}_{SL,B} + \mathbf{v}_B \tag{40}$$

$\mathbf{T}_{CS\text{-}CS3}$ is the transformation matrix between the global coordinate system CS and the local coordinate system CS_3 given as

$$\mathbf{T}_{CS\text{-}CS_3} = \mathrm{rot}_z(\varphi) \cdot \mathrm{rot}_x(\bar{\alpha}) \tag{41}$$

where rot(·) represents a current-frame rotation operation about the axis specified by its subscript, as further described in the Appendix. Angle $\bar{\alpha}$ represents the nominal lead angle of the ball screw given by

$$\bar{\alpha} = \tan^{-1}\left(\frac{\bar{p}}{2\pi\bar{R}_P}\right) \tag{42}$$

Since the screw is fixed, the velocity at the SL contact area on the groove side is zero. Thus, the relative velocity at any point in the SL contact area is

$$\Delta\mathbf{v}_{SL,B} = \mathbf{v}_{SL,B} - \mathbf{0} = \mathbf{v}_{SL,B} \tag{43}$$

The relative velocity expressed in the contact plane (i.e., z_{SL}-y_{SL}) can be formulated as

$$(\Delta\mathbf{v}_{SL,B})_{SL} = \begin{Bmatrix} (\Delta\mathbf{v}_{SL,B})_{SL,y} \\ (\Delta\mathbf{v}_{SL,B})_{SL,z} \end{Bmatrix} = \begin{bmatrix} 0 & 1 & 0 \\ 0 & 0 & 1 \end{bmatrix}(\mathbf{T}_{CS_3\text{-}CS_{SL}})^{-1}(\mathbf{T}_{CS\text{-}CS_3})^{-1}\Delta\mathbf{v}_{SL,B}$$

$$= \begin{Bmatrix} \dfrac{L^2 - 4\pi^2 R_B \bar{R}_P \cos\beta_{SL}}{2\pi L}\omega_B - (\cos\beta_{SL}\omega_z - \sin\beta_{SL}\omega_x)R_B - \left(\left(\dfrac{2\pi\bar{R}_P}{L}\omega_B + \omega_z\right)\sin\beta_{SL} + \omega_x\cos\beta_{SL}\right)z_{SL} \\ R_B\omega_y + \dfrac{R_B\bar{p}}{L}\omega_B + \left(\dfrac{2\pi\bar{R}_P}{L}\omega_B \sin\beta_{SL} + \omega_x\cos\beta_{SL} + \omega_z\sin\beta_{SL}\right)y_{SL} \end{Bmatrix} \tag{44}$$

where

$$L = \sqrt{(2\pi\bar{R}_P)^2 + \bar{p}^2} \tag{45}$$

Let

$$\omega_{SL} \triangleq \left(\frac{2\pi\bar{R}_P}{L}\omega_B + \omega_z\right)\sin\beta_{SL} + \omega_x\cos\beta_{SL}$$

$$c_{SL} \triangleq \frac{\dfrac{L^2 - 4\pi^2 R_B\bar{R}_P\cos\beta_{SL}}{2\pi L}\omega_B - (\cos\beta_{SL}\omega_z - \sin\beta_{SL}\omega_x)R_B}{\omega_{SL}} \tag{46}$$

$$d_{SL} \triangleq -\frac{R_B\omega_y + \dfrac{R_B\bar{p}}{L}\omega_B}{\omega_{SL}}$$

The relative velocity field in Eq. (44) is rewritten as

$$\begin{Bmatrix} (\Delta\mathbf{v}_{SL,B})_{SL,y} \\ (\Delta\mathbf{v}_{SL,B})_{SL,z} \end{Bmatrix} = \begin{Bmatrix} \omega_{SL}(c_{SL} - z_{SL}) \\ \omega_{SL}(-d_{SL} + y_{SL}) \end{Bmatrix} \tag{47}$$

Following the same procedure, the velocity field for other contact areas is derived (see Appendix for details). It is observed that the relative velocity field in the elliptical contact area is a circular contour centered at (c_i, d_i) as shown in Fig. 14, with $i \in \{\text{SL, SR, NR, NL}\}$ representing different contact areas. Note that the center of the contour represents the zero-velocity point.

With the velocity field expressed over the contact area, friction can be calculated given normal contact stress distribution similar to that in linear ball bearings. The frictional force $f_{i,y}$ along y_i-axis and $f_{i,z}$ along z_i-axis, the frictional moment $M_{i,O}$ about the contact center, and friction loss are calculated by double integrating the frictional stress over the contact area. Comparing the relative velocity field of ball screw in Fig. 14 with that of linear ball bearing in Fig. 3, the major difference is that the helix of ball screw introduces relative rotation between the screw and nut about y_3-axis. Thus, there are frictional forces in z_{SL}-direction, which lie in the cross-sectional plane, making frictional forces (from a given contact surface) and normal contact forces (from other contact surfaces) coupled in ball screw. As a result, friction and contact load distribution need to be calculated together in ball screw. The authors have developed a low-order static load distribution model for ball screw [19], including geometric errors and bulk elastic deformations. The model was validated favorably against high-order FE models in ANSYS. Here, it is augmented to include friction.

To calculate contact load distribution, the first step is to describe the geometry of groove surface as a multivariate function. Again, focusing on the SL contact surface, the multivariate function is given by $\mathbf{S}_{SL}(\varphi, \gamma)$ in the CS coordinate system [19], where γ is the cross-sectional angular variable as shown in Fig. 15. Geometric errors such as lead error and contact angle deviation are readily incorporated in $\mathbf{S}_{SL}(\varphi, \gamma)$ [19]. Considering the bulk elastic deformation of the screw $\mathbf{d}_{SL}(\varphi, \gamma)$, the deformed groove surface becomes $\tilde{\mathbf{S}}_{SL}(\varphi, \gamma)$, i.e., $\tilde{\mathbf{S}}_{SL}(\varphi, \gamma) = \mathbf{S}_{SL}(\varphi, \gamma) + \mathbf{d}_{SL}(\varphi, \gamma)$. The authors' prior work [19] detailed the calculation of elastic deformations via a low-order finite element method considering normal contact forces.

At the cross section of the groove with azimuth angle φ_B where the ball is located, the 2D groove surface profile with elastic deformation represented in z_3-x_3 coordinates is given as

$$\tilde{\mathbf{A}}_{SL,2D}(\gamma) = \begin{bmatrix} 1 & 0 & 0 \\ 0 & 0 & 1 \end{bmatrix} \cdot (\text{rot}_z(\varphi_B) \cdot \text{rot}_x(\bar{\alpha}))^{-1} \times (\tilde{\mathbf{S}}_{SL}(\varphi_B, \gamma) - \bar{\mathbf{q}}_B(\varphi_B)) \tag{48}$$

Assume that 2D coordinates of the ball center are $\mathbf{p}_B = \{x_{B3}, z_{B3}\}^T$ and those of the SL contact point are $\mathbf{p}_{SL} = \{x_{SL3}, z_{SL3}\}^T$ in the cross section (i.e., x_3z_3-plane). The following conditions must be satisfied:

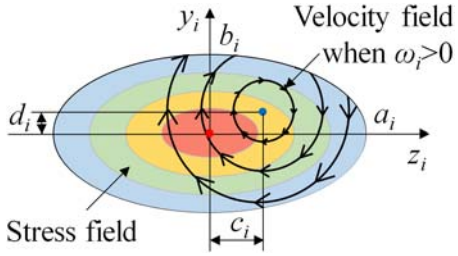

Fig. 14 Contact area and relative velocity field for ball screw

(i) The contact point must lie on the groove surface

$$\mathbf{p}_{SL} = \tilde{\mathbf{A}}_{SL,2D}(\gamma)|_{\gamma=\beta_{SL}} \tag{49}$$

(ii) The contact normal must be perpendicular to the groove surface at the contact point

$$\hat{\mathbf{n}}_{SL} \cdot \hat{\mathbf{m}}_{SL} = 0 \tag{50}$$

where $\hat{\mathbf{n}}_{SL}$ denotes the ball surface contact normal unit vector, pointing from the contact point to the ball center, i.e.,

$$\hat{\mathbf{n}}_{SL} = \frac{\mathbf{p}_B - \mathbf{p}_{SL}}{|\mathbf{p}_B - \mathbf{p}_{SL}|} \tag{51}$$

while $\hat{\mathbf{m}}_{SL}$ represents the groove surface contact normal unit vector as

$$\hat{\mathbf{m}}_{SL} = \left.\frac{d\tilde{\mathbf{A}}_{SL,2D}(\gamma)}{d\gamma}\right|_{\gamma=\beta_{SL}} \tag{52}$$

(iii) The contact force lies along the contact normal and is of magnitude F_{SL}, determined from Hertzian contact theory as

$$F_{SL} = \begin{cases} \left(\frac{1}{C_{SL}}\delta_{SL}\right)^{\frac{3}{2}} & \text{if } \delta_{SL} > 0, \ \delta_{SL} = R_B - |\mathbf{p}_B - \mathbf{p}_{SL}| \\ 0 & \text{if } \delta_{SL} \le 0 \end{cases} \tag{53}$$

where δ_{SL} is the Hertzian contact deformation of the ball surface relative to the groove surface and C_{SL} is Hertzian constant of which calculation can be found in Ref. [19]. Note that the contact model presented here is a 2D version of the 3D contact model in Ref. [19] with azimuth angles set to be φ_B for all the four contact points. It is to keep in accordance with the kinematic analysis in this paper which is done in the cross section.

Neglecting gyroscopic effect, the ball needs to be in quasi-static equilibrium under normal load, frictional force and moment as

$$\sum \begin{pmatrix} \mathbf{F} \\ \mathbf{M} \end{pmatrix}_0 = \begin{bmatrix} \cos\beta_{SL} & \cos\beta_{SR} & -\cos\beta_{NR} & -\cos\beta_{NL} \\ 0 & 0 & 0 & 0 \\ \sin\beta_{SL} & -\sin\beta_{SR} & -\sin\beta_{NR} & \sin\beta_{NL} \\ 0 & 0 & 0 & 0 \\ 0 & 0 & 0 & 0 \\ 0 & 0 & 0 & 0 \end{bmatrix} \begin{Bmatrix} F_{SL} \\ F_{SR} \\ F_{NR} \\ F_{NL} \end{Bmatrix} + \begin{bmatrix} 0 & 0 & 0 & 0 \\ 1 & 1 & 1 & 1 \\ 0 & 0 & 0 & 0 \\ R_B\sin\beta_{SL} & -R_B\sin\beta_{SR} & -R_B\sin\beta_{NR} & R_B\sin\beta_{NL} \\ 0 & 0 & 0 & 0 \\ -R_B\cos\beta_{SL} & -R_B\cos\beta_{SR} & R_B\cos\beta_{NR} & R_B\cos\beta_{NL} \end{bmatrix} \begin{Bmatrix} f_{SL,y} \\ f_{SR,y} \\ f_{NR,y} \\ f_{NL,y} \end{Bmatrix}$$
$$+ \begin{bmatrix} -\sin\beta_{SL} & \sin\beta_{SR} & \sin\beta_{NR} & \sin\beta_{NL} \\ 0 & 0 & 0 & 0 \\ \cos\beta_{SL} & \cos\beta_{SR} & -\cos\beta_{NR} & -\cos\beta_{NL} \\ 0 & 0 & 0 & 0 \\ R_B & R_B & R_B & R_B \\ 0 & 0 & 0 & 0 \end{bmatrix} \begin{Bmatrix} f_{SL,z} \\ f_{SR,z} \\ f_{NR,z} \\ f_{NL,z} \end{Bmatrix} + \begin{bmatrix} 0 & 0 & 0 & 0 \\ 0 & 0 & 0 & 0 \\ 0 & 0 & 0 & 0 \\ \cos\beta_{SL} & \cos\beta_{SR} & -\cos\beta_{NR} & -\cos\beta_{NL} \\ 0 & 0 & 0 & 0 \\ \sin\beta_{SL} & -\sin\beta_{SR} & -\sin\beta_{NR} & \sin\beta_{NL} \end{bmatrix} \begin{Bmatrix} M_{SL,O} \\ M_{SR,O} \\ M_{NR,O} \\ M_{NL,O} \end{Bmatrix} = \begin{Bmatrix} 0 \\ 0 \\ 0 \\ 0 \\ 0 \\ 0 \end{Bmatrix} \tag{54}$$

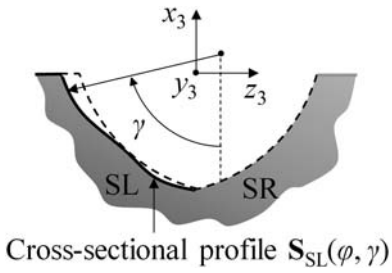

Fig. 15 Cross-sectional profile of ball screw with geometric errors

In summary, a state vector $\mathbf{x} = [\mathbf{p}_{SL}^T, \mathbf{p}_{SR}^T, \mathbf{p}_{NL}^T, \mathbf{p}_{NR}^T, \mathbf{p}_B^T, \gamma_{SL}, \gamma_{SR}, \gamma_{NL}, \gamma_{NR}, \omega_B, \omega_x, \omega_y, \omega_z]^T_{18\times1}$ is defined for each ball together with a function $\mathbf{\Phi}(\mathbf{x})$ containing conditions for quasi-static equilibrium of the ball based on Eqs. (49), (50), and (54) as

$$\mathbf{\Phi}(\mathbf{x}) = \begin{Bmatrix} (\mathbf{p}_{SL} - \tilde{\mathbf{A}}_{SL,2D}(\beta_{SL}))_{2\times1} \\ \vdots \\ \left(\dfrac{\mathbf{p}_B - \mathbf{p}_{SL}}{|\mathbf{p}_B - \mathbf{p}_{SL}|} \cdot \dfrac{d\tilde{\mathbf{A}}_{SL,2D}(\gamma)}{d\gamma}\Big|_{\gamma=\beta_{SL}}\right)_{1\times1} \\ \vdots \\ \sum \begin{pmatrix} \mathbf{F} \\ \mathbf{M} \end{pmatrix}_0 \end{Bmatrix}_{18\times1} = \mathbf{0} \tag{55}$$

The same conditions hold for all the balls.

3.2 Low-Order Numerical Model of Ball-to-Ball Contact.

The orbiting angular velocities of individual balls in ball screw differ depending on contact angles and loading conditions. Similar to linear ball bearing, ball-to-ball contact develops when the orbiting angular velocity of the ball behind is faster than the ball in front ($\omega_{B,10} > \omega_{B,20}$) and when the angular distance between the two balls $\Delta\varphi_{12}$ is close enough ($\Delta\varphi_{12} = \varphi_{B,1} - \varphi_{B,2} \le 2\beta_{B2B}$); β_{B2B} is ball-to-ball contact angle as shown in Fig. 16 and is defined as

$$\beta_{B2B} = \text{asin}\left(\frac{2\pi R_B}{L}\right) \tag{56}$$

Note that the radius for ball-to-ball contact in Fig. 16 is not the pitch circle radius R_P, but L defined in Eq. (45) with the lead of the ball screw factored in.

At the ball-to-ball contact interface between ball 1 and ball 2, another coordinate system CS_4 is established: z_4-x_4 plane is where ball-to-ball contact happens. Similar to the linear ball bearing case, the relative velocity at the ball-to-ball contact interface measured on ball 1 is expressed as

$$\begin{Bmatrix} (\Delta\mathbf{v}_{B2B})_{z_4} \\ (\Delta\mathbf{v}_{BL})_{x_4} \end{Bmatrix} = \begin{Bmatrix} (\omega_{x,1} + \omega_{x,2})R_B \cos\beta_{B2B} + (\omega_{y,1} - \omega_{y,2})R_B \sin\beta_{B2B} \\ -(\omega_{z,1} + \omega_{z,2})R_B \end{Bmatrix} \tag{57}$$

Denoting the normal contact force at the ball-to-ball contact interface as F_{B2B} (i.e., in y_4-direction), the ball-to-ball contact frictional force in the contact interface (z_4-x_4 plane) is

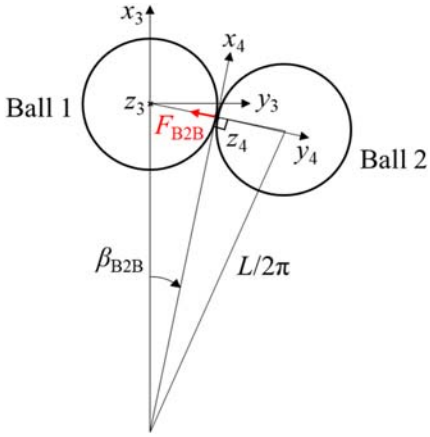

Fig. 16 Ball-to-ball contact between two balls in ball screw

$$\begin{Bmatrix} f_{B2B,z_4} \\ f_{B2B,x_4} \end{Bmatrix} = \begin{Bmatrix} -(\Delta\mathbf{v}_{B2B})_{z_4}/|\Delta\mathbf{v}_{B2B}| \cdot \mu F_{B2B} \\ -(\Delta\mathbf{v}_{B2B})_{x_4}/|\Delta\mathbf{v}_{B2B}| \cdot \mu F_{B2B} \end{Bmatrix}, \quad |\Delta\mathbf{v}_{B2B}| = \sqrt{(\Delta\mathbf{v}_{B2B})_{z_4}^2 + (\Delta\mathbf{v}_{B2B})_{x_4}^2} \tag{58}$$

Under ball-to-ball contact, ball 1 needs to be in quasi-static equilibrium with the addition of ball-to-ball contact force and friction to Eq. (54) as

$$\sum \begin{pmatrix} \mathbf{F} \\ \mathbf{M} \end{pmatrix}_0 + \begin{bmatrix} \sin\beta_{B2B} & 0 & \cos\beta_{B2B} \\ -\cos\beta_{B2B} & 0 & \sin\beta_{B2B} \\ 0 & 1 & 0 \\ 0 & R_B\cos\beta_{B2B} & 0 \\ 0 & R_B\sin\beta_{B2B} & 0 \\ 0 & 0 & -R_B \end{bmatrix} \times \begin{Bmatrix} F_{B2B} \\ f_{B2B,z_4} \\ f_{B2B,x_4} \end{Bmatrix} = \begin{Bmatrix} 0 \\ 0 \\ 0 \\ 0 \\ 0 \\ 0 \end{Bmatrix} \tag{59}$$

Similar equations hold for ball 2, only that ball-to-ball contact force and friction are in the opposite direction.

Besides satisfying their own quasi-static equilibrium, the two balls need to satisfy ball-to-ball contact conditions: if the two balls are in contact, then they need to move at the same orbiting angular velocity at quasi-static states; otherwise, the ball-to-ball contact force is 0.

$$\begin{cases} \omega_{B,1} = \omega_{B,2}, & \text{if } \omega_{B,10} \ge \omega_{B,20} \text{ and } \Delta\varphi_{12} = \varphi_1 - \varphi_2 \le 2\beta_{B2B} \\ F_{B2B} = 0, & \text{otherwise} \end{cases} \tag{60}$$

Put together Eq. (59) for quasi-static equilibrium of ball 1, similar equations for ball 2 and Eq. (60) for ball-to-ball contact, the motion of two balls and ball-to-ball contact force (if there is any) are determined. Upon solution, ball-to-ball contact friction and loss are calculated accordingly.

Similar to that in linear ball bearings, ball-to-ball contact between two balls in ball screws can be generalized to multi-ball-to-ball contact as

$$\begin{cases} \text{Quasi-static equilibrium for ball } j \\ \text{B2B contact between ball } j \text{ and } j+1: \begin{cases} \omega_{B,j} = \omega_{B,(j+1)}, & \text{if } \omega_{B,j0} \ge \omega_{B,(j+1)0} \text{ and } \varphi_j - \varphi_{j+1} \le 2\beta_{B2B} \\ F_{B2B,j} = 0, & \text{otherwise} \end{cases} \end{cases} \tag{61}$$

3.3 Finite Element Analysis Validation of Ball-to-Ball Contact Model. To validate the low-order numerical model of ball-to-ball contact for ball screws, the results are compared with those from ANSYS FEA in the same ball-to-ball contact module between two balls as shown in Fig. 12. The reasons for validation in the two-ball module instead of the whole ball screw are: (1) ball-to-ball contact modeling is the main focus of this work, thus validation of ball-to-ball contact is the priority and (2) the dynamic simulation of a full ball screw with enough accuracy is computationally too demanding.

Parameters for ball screw used in this validation study are shown in Table 4. The geometry and material properties are the same as those in the authors' prior work for static load distribution [19]. The groove profile on the screw side has contact angle deviation θ as shown in Fig. 17. Two cases are simulated to demonstrate the effect of different contact angle deviation: $\theta = 0$ deg is set for ball 1 in both cases; for ball 2, $\theta = 2$ deg is set in case (a) and $\theta = 3$ deg is used in case (b). This kind of contact angle deviation induces different orbiting angular velocities of balls and results in ball-to-ball contact in both cases (a) and (b).

As a benchmark, dynamic simulation of ball-to-ball contact in ball screw is conducted in ANSYS Workbench 16.2. The CAD model of the two-ball module for case (a) is shown in Fig. 18, which are meshed with tetrahedral elements of size 0.05 mm around the contact area and 1 mm elsewhere, giving the FE model 230,816 elements in total. Mesh refinement of size 0.05 mm is picked after mesh sensitivity analysis. Similarly, the FEA model of case (b) has 231,931 elements. The ball nut is made to rotate about the ball screw axis at ω_N. The screw shaft is constrained by frictionless support to only translate along the axial direction with external force 50 N in both cases. The two balls are placed at an initial distance of 1 μm apart to accelerate ball-to-ball contact. A total simulation time of 0.005 s is split into ten time steps to simulate the dynamic process from no ball-to-ball contact to the development of ball-to-ball contact and finally stabilized ball-to-ball contact under quasi-static equilibrium. The other important settings in ANSYS FEA are kept the same as in the linear ball bearing case in Sec. 2.5. The contact problem is solved using the same desktop computer as used for the linear ball bearing case study.

Table 4 Parameters for ball-to-ball contact simulation in ball screw

Parameter (symbol)	Value (unit)
Ball radius (R_B)	2.778 (mm)
Conformity ratio of groove (conf.)	0.56
Pitch radius of ball screw (R_P)	16.5 (mm)
Lead of ball screw (p)	20 (mm)
Nominal contact angle (β_0)	45 (deg)
Angular velocity of the nut (ω_N)	2π (rad/s)
Friction coefficient of metal-to-metal contact (μ)	0.1
Young's modulus	210 (N/mm^2)
Poisson's ratio	0.28

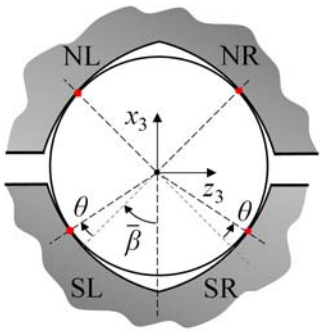

Fig. 17 Contact angle deviation at the cross section of ball screw grooves

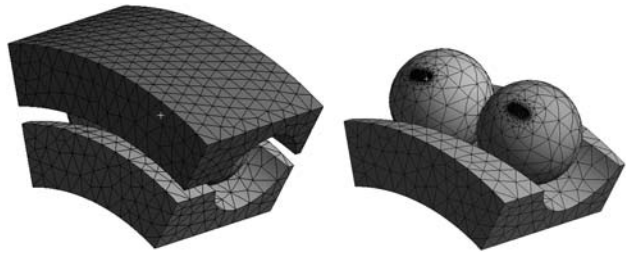

Fig. 18 Mesh for ball screw in ANSYS

The ball-to-ball contact forces from the low-order numerical model and ANSYS FEA are compared in Table 5. It is observed that ball-to-ball contact forces predicted by the low-order numerical model are reasonably close to those from ANSYS FEA, with 6.67% and 6.64% difference for cases (a) and (b), respectively. As shown in the comparison of computational time in Table 3, the low-order numerical model is three orders of magnitude faster than ANSYS FEA, indicating the computational efficiency of the proposed low-order model once again. For case (a), the friction increase caused by ball-to-ball contact is 39.2% relative to that before ball-to-ball contact, according to the low-order numerical model, while 60.2% friction increase is observed for case (b). Both results indicate the significance of ball-to-ball contact to the friction increase of ball screw.

3.4 Simulation of a Whole Ball Screw With Ball-to-Ball Contact. Since the proposed low-order numerical model of ball-to-ball contact in ball screw has been validated, it can be incorporated in the whole ball screw friction model to simulate the friction behavior of the whole ball screw. A ball screw with the same parameters as shown in Table 4 is used in the simulation. The ball screw is 800 mm long with the nut initially placed in the middle. A total time of 2 s in 200 steps are simulated. The nut is confined to only rotate, while screw shaft is only allowed to translate in the axial direction at the two ends. The axial load of 1500 N is applied to the screw shaft on one end, and 37 balls in two loaded turns yield 97.8% occupation ratio of the active ball track. Recirculation of balls is modeled by connecting the start and end of the return tube. The same type of contact angle deviation in Fig. 17 is adopted; the magnitude of contact angle deviation θ on the screw side is set to be sinusoidal with respect to azimuth angle as shown in Fig. 19.

The balls are evenly distributed at the start of the simulation. However, due to the sinusoidal contact angle deviation, the orbiting angular velocities of the balls differ, making the distance between balls to change over time. Figure 20 shows the angular distance between balls with respect to the nut rotation angle (i.e., which is proportional to time); balls in ball-to-ball contact are marked as black dots. Four groups of ball-to-ball contact form because of the velocity difference induced by the four cycles of contact angle deviations in Fig. 19.

Table 5 Comparison of ball-to-ball contact forces and computational time based on low-order numerical model and ANSYS FEA for ball screw

		Low-order numerical model	ANSYS FEA
Case (a)	B2B contact force (N)	1.92	1.80
	Computational time	15.3 s	5.75 h
Case (b)	B2B contact force (N)	2.89	2.71
	Computational time	14.7 s	5.35 h

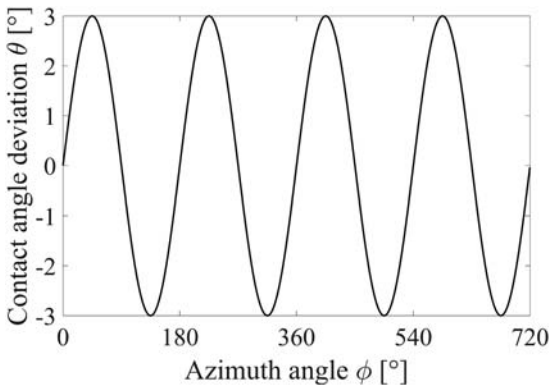

Fig. 19 Contact angle deviation with respect to azimuth angle

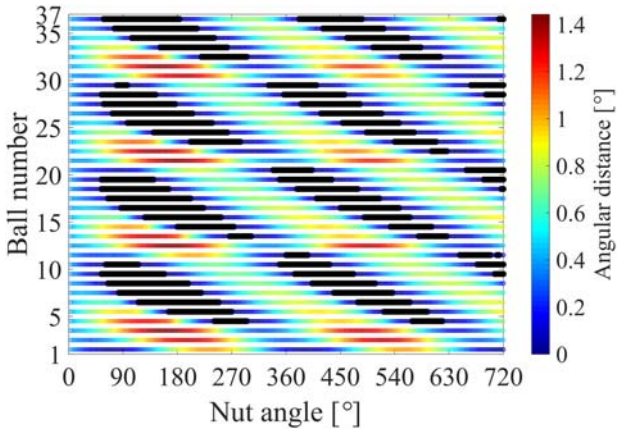

Fig. 20 Angular distance between the balls and ball-to-ball contact status (ball-to-ball contact is marked using black dots)

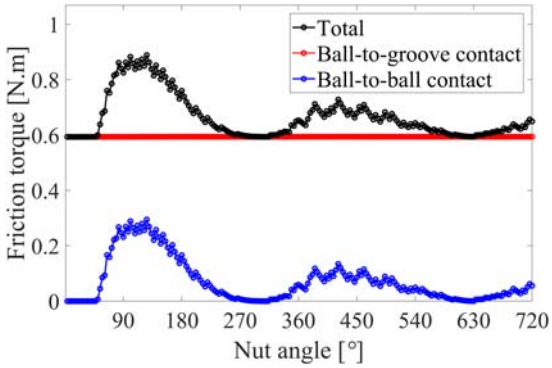

Fig. 21 Total friction torque and the contribution of ball-to-groove and ball-to-ball contact

Figure 21 shows the total friction torque and the contribution of ball-to-groove and ball-to-ball contact. It is observed that ball-to-groove contact friction barely has variation in this case study, while ball-to-ball contact contributes to a maximum of 49.6% additional friction torque at 126 deg nut rotation angle. As the contacted balls gradually disengage, the friction torque contributed by ball-to-ball contact decreases and reaches its minimum value 0 at 306 deg nut rotation angle when there is no ball-to-ball contact. After that, ball-to-ball contact builds up again and gradually stabilizes. Thus, ball-to-ball contact not only gives rise to a significant friction increase but also significant friction variation due to the engagement and disengagement of ball-to-ball contact.

4 Conclusion and Future Work

The modeling of ball-to-ball contact friction is very important to the rolling element machine components like linear ball bearings and ball screws. In this paper, low-order numerical models for ball-to-ball contact friction in linear ball bearings and ball screws are developed. Furthermore, an analytical model for ball-to-ball contact friction in four-point contact linear ball bearing is derived by making simplifications to its low-order numerical model. Compared with ball-to-ball friction predictions from FEA models developed in ANSYS, the proposed numerical models are shown in case studies to be accurate within 7%, while computing at least three orders of magnitude faster. Using the insights gained from the analytical model, ball-to-ball contact is shown to be mitigated by reducing the velocity difference of balls in four-point contact linear ball bearings. Significant friction increase and variation due to ball-to-ball contact are demonstrated in a case study of ball screw, highlighting the importance of modeling ball-to-ball contact. The proposed ball-to-ball contact models are useful for the analysis and design optimization of linear ball bearings and ball screws. Based on the developed model, simulation-based case studies can be conducted to find out the effect of different geometric errors on ball-to-ball contact-induced friction. Coulomb friction model is used in the developed model, and more detailed formulation with a lubrication effect can be conducted in the future. Effects of the return tube can also be incorporated into the model in future work.

Acknowledgment

This work is funded in part by a research gift from the Ford Motor Company. The authors would like to thank Dr. Jason S. Wou from the Ford Motor Company for bringing up the problem of ball-to-ball contact and his valuable feedback during the development of the ball-to-ball contact model.

Nomenclature

a = length of the semi-major axis of the elliptical contact area
b = length of the semi-minor axis of the elliptical contact area
c = location of the velocity center along the semi-major axis
d = location of the velocity center along the semi-minor axis
p = lead of ball screw
r = radius
v = magnitude of translational velocity
$\mathbf{d}$ = 3D deformation of the groove surface
$\mathbf{m}$ = normal of groove surface
$\mathbf{n}$ = normal direction
$\mathbf{p}$ = coordinates of a contact point or ball center
$\mathbf{q}$ = vector of position
$\mathbf{v}$ = translational velocity vector
$\mathbf{x}$ = state vector of unknown variables
E = Young's modulus
F = magnitude of force
M = magnitude of a moment
$\mathbf{A}$ = 2D groove surface function in the local coordinate system
$\mathbf{F}$ = generalized force vector
$\mathbf{M}$ = generalized moment vector
$\mathbf{S}$ = 3D groove surface function in the global coordinate system
$\mathbf{T}$ = transformation matrix
r_g = gear ratio of ball screw
R_P = pitch circle radius of ball screw
B2B = ball-to-ball contact

CS = coordinate system
Ellip(·) = complete elliptic integral of the second kind
rot(·) = current frame rotation operator
sgn(·) = sign of a variable
α = lead angle of ball screw
β = contact angle of ball screw
γ = cross-sectional angular variable
δ = Hertzian deformation
ε = velocity difference
ζ = additional angular deviation caused by ball-to-ball contact
η = angular deviation of the velocity center from the contact center
θ = contact angle deviation
μ = friction coefficient
ν = Poisson's ratio
ρ = side force ratio
φ = angular distance traversed along the nominal ball center pathway about screw/nut's axis (azimuth angle) of ball screw
$\mathbf{\Phi}$ = objective function
Ψ = constant related to Hertzian contact
ω = magnitude of angular velocity
$\boldsymbol{\omega}$ = angular velocity vector of the ball screw
$\boldsymbol{\Omega}$ = angular velocity vector of linear ball bearing

Subscripts and Superscripts

B = parameter pertaining to the balls
BL = parameter pertaining to the bottom left surface of linear ball bearing
BR = parameter pertaining to the bottom right surface of linear ball bearing
G = parameter pertaining to the groove
i = variable for contact point
j = ball number
NL = parameter pertaining to nut left surface of ball screw
NR = parameter pertaining to nut right surface of ball screw
S = parameter pertaining to the screw shaft
SL = parameter pertaining to screw left surface of ball screw
SR = parameter pertaining to screw right surface of ball screw
T = transpose of a matrix or vector
TL = parameter pertaining to the top left surface of linear ball bearing
TR = parameter pertaining to the top right surface of linear ball bearing
x, y, and z = parameters pertaining to the x, y, and z directions, respectively

Accents

$\hat{\cdot}$ = normalized vector
$\bar{\cdot}$ = nominal value
$\dot{\cdot}$ = derivative
$\tilde{\mathrm{S}}$ = deformed surface

Appendix

Velocity Field at the BR, TR, and TL Contact Areas in Linear Ball Bearing

$$\begin{Bmatrix} (\Delta\mathbf{v}_{\mathrm{BR,B}})_{\mathrm{BR},x} \\ (\Delta\mathbf{v}_{\mathrm{BR,B}})_{\mathrm{BR},z} \end{Bmatrix} = \begin{Bmatrix} \omega_{\mathrm{BR}}(-d_{\mathrm{BR}} + z_{\mathrm{BR}}) \\ \omega_{\mathrm{BR}}(c_{\mathrm{BR}} - x_{\mathrm{BR}}) \end{Bmatrix} = \begin{Bmatrix} (-\omega_x \sin\beta_{\mathrm{BR}} + \omega_y \cos\beta_{\mathrm{BR}})z_{\mathrm{BR}} \\ v_{\mathrm{B}} - (\omega_x \cos\beta_{\mathrm{BR}} + \omega_y \sin\beta_{\mathrm{BR}})R_{\mathrm{B}} - (-\omega_x \sin\beta_{\mathrm{BR}} + \omega_y \cos\beta_{\mathrm{BR}})x_{\mathrm{BR}} \end{Bmatrix} \tag{A1}$$

$$\begin{Bmatrix} (\Delta\mathbf{v}_{\mathrm{TR,B}})_{\mathrm{TR},x} \\ (\Delta\mathbf{v}_{\mathrm{TR,B}})_{\mathrm{TR},z} \end{Bmatrix} = \begin{Bmatrix} \omega_{\mathrm{TR}}(-d_{\mathrm{TR}} + z_{\mathrm{TR}}) \\ \omega_{\mathrm{TR}}(c_{\mathrm{TR}} - x_{\mathrm{TR}}) \end{Bmatrix} = \begin{Bmatrix} (-\omega_x \sin\beta_{\mathrm{TR}} - \omega_y \cos\beta_{\mathrm{TR}})z_{\mathrm{TR}} \\ v_{\mathrm{B}} - v + (\omega_x \cos\beta_{\mathrm{TR}} - \omega_y \sin\beta_{\mathrm{TR}})R_{\mathrm{B}} - (-\omega_x \sin\beta_{\mathrm{TR}} - \omega_y \cos\beta_{\mathrm{TR}})x_{\mathrm{TR}} \end{Bmatrix} \tag{A2}$$

$$\begin{Bmatrix} (\Delta\mathbf{v}_{\mathrm{TL,B}})_{\mathrm{TL},x} \\ (\Delta\mathbf{v}_{\mathrm{TL,B}})_{\mathrm{TL},z} \end{Bmatrix} = \begin{Bmatrix} \omega_{\mathrm{TL}}(-d_{\mathrm{TL}} + z_{\mathrm{TL}}) \\ \omega_{\mathrm{TL}}(c_{\mathrm{TL}} - x_{\mathrm{TL}}) \end{Bmatrix} = \begin{Bmatrix} (\omega_x \sin\beta_{\mathrm{TL}} - \omega_y \cos\beta_{\mathrm{TL}})z_{\mathrm{TL}} \\ v_{\mathrm{B}} - v + (\omega_x \cos\beta_{\mathrm{TL}} + \omega_y \sin\beta_{\mathrm{TL}})R_{\mathrm{B}} - (\omega_x \sin\beta_{\mathrm{TL}} - \omega_y \cos\beta_{\mathrm{TL}})x_{\mathrm{TL}} \end{Bmatrix} \tag{A3}$$

Frictional Force, Frictional Moment, and Frictional Loss in the Contact Area of a Linear Ball Bearing

Frictional force $f_{i,z}$ along z_i-axis, frictional moment $M_{i,O}$ about contact center, and frictional loss P_{fi} measured in power in the contact area of a linear ball bearing are calculated by the double integral of the frictional stress over the contact area with Hertzian contact stress distribution

$$\begin{aligned} f_{i,z} &= \mathrm{sgn}(\omega_i)\iint_D \mu\sigma_{i,0}\left(1 - \frac{x_i^2}{a_i^2} - \frac{z_i^2}{b_i^2}\right)^{1/2} \frac{x_i - c_i}{\sqrt{(x_i - c_i)^2 + z_i^2}} dx_i dz_i \\ &= \mathrm{sgn}(\omega_i)a_i b_i \mu\sigma_{i,0}\iint_D (1 - t^2 - s^2)^{1/2} \frac{t - c_i/a_i}{\sqrt{(t - c_i/a_i)^2 + (b_i/a_i \cdot s)^2}} dsdt \left(t = \frac{x_i}{a_i}, s = \frac{z_i}{b_i}, D{:}t^2 + s^2 \le 1\right) \\ &= \mathrm{sgn}(\omega_i)a_i b_i \mu\sigma_{i,0}\int_0^{2\pi}\int_0^1 (1 - r^2)^{1/2} \frac{r\cos\theta - c_i/a_i}{\sqrt{(r\cos\theta - c_i/a_i)^2 + (b_i/a_i \cdot r\sin\theta)^2}} rdrd\theta\,(r\cos\theta = t,\ r\sin\theta = s) \end{aligned} \tag{A4}$$

$$
\begin{aligned}
M_{i,O} &= \mathrm{sgn}(\omega_i)\iint_D \mu\sigma_{i,0}\left(1-\frac{x_i^2}{a_i^2}-\frac{z_i^2}{b_i^2}\right)^{1/2}\left(\frac{x_i-c_i}{\sqrt{(x_i-c_i)^2+z_i^2}}x_i-\frac{-z_i}{\sqrt{(x_i-c_i)^2+z_i^2}}z_i\right)dx_idz_i \\
&= \mathrm{sgn}(\omega_i)a_i^2b_i\mu\sigma_{i,0}\iint_D (1-t^2-s^2)^{1/2}\left(\frac{t^2-c_i/a_it+b_i^2/a_i^2s^2}{\sqrt{(t-c_i/a_i)^2+(b_i/a_i\cdot s)^2}}\right)dsdt\ \left(t=\frac{x_i}{a_i},\ s=\frac{z_i}{b_i},\ D{:}t^2+s^2\le 1\right) \\
&= \mathrm{sgn}(\omega_i)a_i^2b_i\mu\sigma_{i,0}\int_0^{2\pi}\int_0^1 (1-r^2)^{1/2}\left(\frac{r^2\cos\theta^2-c_i/a_ir\cos\theta+b_i^2/a_i^2r^2\sin\theta^2}{\sqrt{(r\cos\theta-c_i/a_i)^2+(b_i/a_i\cdot r\sin\theta)^2}}\right)rdrd\theta\,(r\cos\theta=t,\ r\sin\theta=s)
\end{aligned}
\tag{A5}
$$

$$
\begin{aligned}
P_{fi} &= |\omega_i|\iint_D \mu\sigma_{i,0}\left(1-\frac{x_i^2}{a_i^2}-\frac{z_i^2}{b_i^2}\right)^{1/2}\sqrt{(x_i-c_i)^2+z_i^2}dx_idz_i \\
&= |\omega_i|a_i^2b_i\mu\sigma_{i,0}\iint_D (1-t^2-s^2)^{1/2}\sqrt{(t-c_i/a_i)^2+(b_i/a_i\cdot s)^2}dsdt\ \left(t=\frac{x_i}{a_i},\ s=\frac{z_i}{b_i},\ D{:}t^2+s^2\le 1\right) \\
&= |\omega_i|a_i^2b_i\mu\sigma_{i,0}\int_0^{2\pi}\int_0^1 (1-r^2)^{1/2}\sqrt{(r\cos\theta-c_i/a_i)^2+(b_i/a_i\cdot r\sin\theta)^2}\,rdrd\theta\ (t=r\cos\theta,\ s=r\sin\theta)
\end{aligned}
\tag{A6}
$$

where $\sigma_{i,0}$ is the maximum contact pressure and is determined by normal contact force F_i as

$$
\sigma_{i,0}=\frac{3F_i}{2\pi a_ib_i} \tag{A7}
$$

Magnitude of $\Delta\eta_i$ for the Linearized Region of Frictional Force

The magnitude of angular deviation $\Delta\eta_i$ in Eq. (13) is decomposed as

$$
|\Delta\eta_i|=\left|\frac{c_i}{R_B}\right|=\left|\frac{c_i}{a_i}\right|\cdot\left|\frac{a_i}{R_B}\right| \tag{A8}
$$

In order for linear approximation of frictional force to be valid, $|c_i/a_i|<0.5$ has to be satisfied as shown in Fig. 5. The ratio of the semimajor axis a_i to the ball radius R_B depends on the normal contact load F_i (or maximum contact stress σ_i over the contact area) and the conformity ratio of the groove. Figure 22 plots a_i/R_B as a function of σ_i with four typical conformity ratios of ball bearings. The plot is cut off at maximum allowable stress of 1554 MPa for Hertzian contact, which is 4.2 times of typical carbon steel's yield strength (370 MPa) according to Ref. [22].

The maximum value of a_i/R_B is 0.218 achieved at the maximum allowable stress with conf. = 0.52. The higher the conformity ratio, the smaller the a_i/R_B; a_i/R_B also decreases with contact stress (or contact load). In the worst-case scenario, $|\Delta\eta_i|<0.5\times0.218=0.109$, which is equivalent of 6.25 deg.

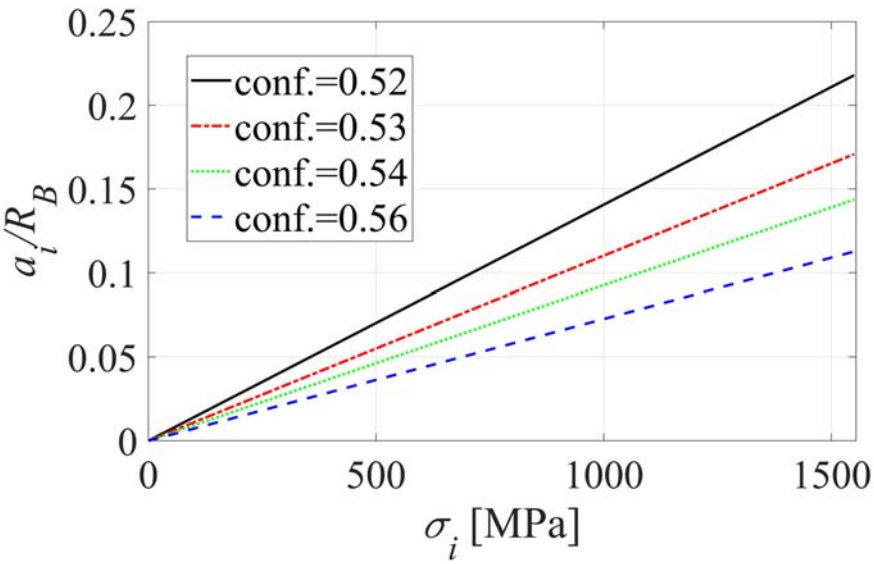

Fig. 22 The ratio of the semimajor axis a_i to the ball radius R_B

Current Frame Rotation Matrices

The rotation operator $\mathrm{rot}_{x/z}(\theta)$ performs a rotation of angle θ around x/z-axis. Their elements are given as

$$\mathrm{rot}_x(\theta) = \begin{bmatrix} 1 & 0 & 0 \\ 0 & \cos\theta & -\sin\theta \\ 0 & \sin\theta & \cos\theta \end{bmatrix}, \quad \mathrm{rot}_z(\theta) = \begin{bmatrix} \cos\theta & -\sin\theta & 0 \\ \sin\theta & \cos\theta & 0 \\ 0 & 0 & 1 \end{bmatrix}$$

Velocity Field at the SR, NR, and NL Contact Areas in Ball Screw

$$(\Delta\mathbf{v}_{\mathrm{SR,B}})_{\mathrm{SR}} = \begin{Bmatrix} (\Delta\mathbf{v}_{\mathrm{SR,B}})_{\mathrm{SR},y} \\ (\Delta\mathbf{v}_{\mathrm{SR,B}})_{\mathrm{SR},z} \end{Bmatrix} = \begin{Bmatrix} \omega_{\mathrm{SR}}(c_{\mathrm{SR}} + z_{\mathrm{SR}}) \\ \omega_{\mathrm{SR}}(d_{\mathrm{SR}} - y_{\mathrm{SR}}) \end{Bmatrix}$$
$$= \begin{Bmatrix} \dfrac{L^2 - 4\pi^2 R_{\mathrm{B}}\bar{R}_{\mathrm{P}}\cos\beta_{\mathrm{SR}}}{2\pi L}\omega_{\mathrm{B}} - (\cos\beta_{\mathrm{SR}}\omega_z + \sin\beta_{\mathrm{SR}}\omega_x)R_{\mathrm{B}} + \left(\left(\dfrac{2\pi\bar{R}_{\mathrm{P}}}{L}\omega_{\mathrm{B}} + \omega_z\right)\sin\beta_{\mathrm{SR}} - \cos\beta_{\mathrm{SR}}\omega_x\right)z_{\mathrm{SR}} \\ R_{\mathrm{B}}\omega_y + \dfrac{R_{\mathrm{B}}\bar{p}}{L}\omega_{\mathrm{B}} - \left(\dfrac{2\pi\bar{R}_{\mathrm{P}}}{L}\omega_{\mathrm{B}}\sin\beta_{\mathrm{SR}} - \cos\beta_{\mathrm{SR}}\omega_x + \sin\beta_{\mathrm{SR}}\omega_z\right)y_{\mathrm{SR}} \end{Bmatrix} \tag{A9}$$

$$(\Delta\mathbf{v}_{\mathrm{NR}})_{\mathrm{NR}} = \begin{Bmatrix} (\Delta\mathbf{v}_{\mathrm{NR,B}})_{\mathrm{NR},y} \\ (\Delta\mathbf{v}_{\mathrm{NR,B}})_{\mathrm{NR},z} \end{Bmatrix} = \begin{Bmatrix} \omega_{\mathrm{NR}}(c_{\mathrm{NR}} + z_{\mathrm{NR}}) \\ \omega_{\mathrm{NR}}(d_{\mathrm{NR}} - y_{\mathrm{NR}}) \end{Bmatrix}$$
$$= \begin{Bmatrix} \dfrac{L^2 + 4\pi^2 R_{\mathrm{B}}\bar{R}_{\mathrm{P}}\cos\beta_{\mathrm{NR}}}{2\pi L}(\omega_{\mathrm{B}} - \omega_{\mathrm{N}}) + (\cos\beta_{\mathrm{NR}}\omega_z - \sin\beta_{\mathrm{NR}}\omega_x)R_{\mathrm{B}} + \left(\left(\dfrac{2\pi\bar{R}_{\mathrm{P}}}{L}(\omega_{\mathrm{B}} - \omega_{\mathrm{N}}) + \omega_z\right)\sin\beta_{\mathrm{NR}} + \omega_x\cos\beta_{\mathrm{NR}}\right)z_{\mathrm{NR}} \\ R_{\mathrm{B}}\omega_y + \dfrac{R_{\mathrm{B}}\bar{p}}{L}(\omega_{\mathrm{B}} - \omega_{\mathrm{N}}) - \left(\dfrac{2\pi\bar{R}_{\mathrm{P}}}{L}(\omega_{\mathrm{B}} - \omega_{\mathrm{N}})\sin\beta_{\mathrm{NR}} + \omega_x\cos\beta_{\mathrm{NR}} + \omega_z\sin\beta_{\mathrm{NR}}\right)y_{\mathrm{NR}} \end{Bmatrix} \tag{A10}$$

$$(\Delta\mathbf{v}_{\mathrm{NL}})_{\mathrm{NL}} = \begin{Bmatrix} (\Delta\mathbf{v}_{\mathrm{NL,B}})_{\mathrm{NL},y} \\ (\Delta\mathbf{v}_{\mathrm{NL,B}})_{\mathrm{NL},z} \end{Bmatrix} = \begin{Bmatrix} \omega_{\mathrm{NL}}(c_{\mathrm{NL}} - z_{\mathrm{NL}}) \\ \omega_{\mathrm{NL}}(d_{\mathrm{NL}} + y_{\mathrm{NL}}) \end{Bmatrix}$$
$$= \begin{Bmatrix} \dfrac{L^2 + 4\pi^2 R_{\mathrm{B}}\bar{R}_{\mathrm{P}}\cos\beta_{\mathrm{NL}}}{2\pi L}(\omega_{\mathrm{B}} - \omega_{\mathrm{N}}) + (\cos\beta_{\mathrm{NL}}\omega_z + \sin\beta_{\mathrm{NL}}\omega_x)R_{\mathrm{B}} - \left(\left(\dfrac{2\pi\bar{R}_{\mathrm{P}}}{L}(\omega_{\mathrm{B}} - \omega_{\mathrm{N}}) + \omega_z\right)\sin\beta_{\mathrm{NL}} - \omega_x\cos\beta_{\mathrm{NL}}\right)z_{\mathrm{NL}} \\ R_{\mathrm{B}}\omega_y + \dfrac{R_{\mathrm{B}}\bar{p}}{L}(\omega_{\mathrm{B}} - \omega_{\mathrm{N}}) + \left(\dfrac{2\pi\bar{R}_{\mathrm{P}}}{L}(\omega_{\mathrm{B}} - \omega_{\mathrm{N}})\sin\beta_{\mathrm{NL}} - \omega_x\cos\beta_{\mathrm{NL}} + \omega_z\sin\beta_{\mathrm{NL}}\right)y_{\mathrm{NL}} \end{Bmatrix} \tag{A11}$$

References

[1] Hong, S., and Tong, V.-C., 2016, "Rolling-Element Bearing Modeling: A Review," Int. J. Precis. Eng. Manuf., **17**(12), pp. 1729–1749.
[2] Halpin, J. D., and Tran, A. N., 2016, "An Analytical Model of Four-Point Contact Rolling Element Ball Bearings," ASME J. Tribol., **138**(3), p. 031404.
[3] Jones, A. B., 1959, "Ball Motion and Sliding Friction in Ball Bearings," J. Basic Eng., **81**(3), p. 1.
[4] Hamrock, B. J., 1975, "Ball Motion and Sliding Friction in an Arched Outer Race Ball Bearing," ASME J. Lubr. Technol., **97**(2), pp. 202–210.
[5] Harris, T. A., and Kotzalas, M. N., 2006, *Advanced Concepts of Bearing Technology: Rolling Bearing Analysis*, CRC Press, Boca Raton, FL.
[6] Leblanc, A., and Nelias, D., 2007, "Ball Motion and Sliding Friction in a Four-Contact-Point Ball Bearing," ASME J. Tribol., **129**(4), pp. 801–808.
[7] Joshi, A., Kachhia, B., Kikkari, H., Sridhar, M., and Nelias, D., 2015, "Running Torque of Slow Speed Two-Point and Four-Point Contact Bearings," Lubricants, **3**(2), pp. 181–196.
[8] Lin, M. C., Ravani, B., and Velinsky, S. A., 1994, "Kinematics of the Ball Screw Mechanism," ASME J. Mech. Des., **116**(3), pp. 849–855.
[9] Wei, C. C., and Lin, J. F., 2003, "Kinematic Analysis of the Ball Screw Mechanism Considering Variable Contact Angles and Elastic Deformations," ASME J. Mech. Des., **125**(4), pp. 717–733.
[10] Wei, C. C., Lin, J. F., and Horng, J. H., 2009, "Analysis of a Ball Screw With a Preload and Lubrication," Tribol. Int., **42**(11–12), pp. 1816–1831.
[11] Xu, N., Tang, W., Chen, Y., Bao, D., and Guo, Y., 2015, "Modeling Analysis and Experimental Study for the Friction of a Ball Screw," Mech. Mach. Theory, **87**, pp. 57–69.
[12] Heras, I., Aguirrebeitia, J., Abasolo, M., and Plaza, J., 2017, "Friction Torque in Four-Point Contact Slewing Bearings: Applicability and Limitations of Current Analytical Formulations," Tribol. Int., **115**, pp. 59–69.
[13] Lin, B., Duan, M., Okwudire, C. E., and Wou, J. S., 2017, "A Simplified Analytical Model for Rolling/Sliding Behavior and Friction in Four-Point-Contact Ball Bearings and Screws," Proceedings of the ASME 2017 International Mechanical Engineering Congress and Exposition, Tampa, FL, Nov. 3–9.
[14] Zhou, C. G., Feng, H. T., Chen, Z. T., and Ou, Y., 2016, "Correlation Between Preload and No-Load Drag Torque of Ball Screws," Int. J. Mach. Tools Manuf., **102**, pp. 35–40.
[15] Shimoda, H., and Izawa, M., 1987, "Characteristics of Oscillatory Ball Screws (1st Report, Oscillatory Friction Torque of Preloaded Ball Screws with Shim Plates)," Trans. Japan Soc. Mech. Eng. Ser. C, **53**(491), pp. 1495–1499.
[16] Ohta, H., Hanaoka, G., and Ueki, Y., 2017, "Sticking of a Linear-Guideway Type Recirculating Ball Bearing," ASME J. Tribol., **139**(3), p. 031103.
[17] Logan, W., 2018, "The Benefits of Caged Balls: Boosted Lifetime and Reduced Noise," Mach. Des. https://www.machinedesign.com/motion-control/benefits-caged-balls-boosted-lifetime-and-reduced-noise.
[18] Lin, B., Duan, M., Okwudire, C. E., and Wou, J. S., 2018, "An Improved Analytical Model of Friction and Ball Motion in Linear Ball Bearings—With Application to Ball-to-Ball Contact Prediction," Proceedings of the ASME 2018 International Mechanical Engineering Congress and Exposition., Pittsburgh, PA, Nov. 9–15.
[19] Lin, B., Okwudire, C. E., and Wou, J. S., 2018, "Low Order Static Load Distribution Model for Ball Screw Mechanisms Including Effects of Lateral Deformation and Geometric Errors," ASME J. Mech. Des., **140**(2), p. 022301.
[20] Johnson, K. L., 1985, *Contact Mechanics*, Cambridge University Press, Cambridge, UK.
[21] ANSYS Inc., 2010, "Introduction to Contact: ANSYS Mechanical Structural Nonlinearities."
[22] Kogut, L., and Etsion, I., 2002, "Elastic-Plastic Contact Analysis of a Sphere and a Rigid Flat," ASME J. Appl. Mech., **69**(5), pp. 657–662.